Přírodovědecká fakulta
UNIVERZITY KARLOVY V PRAZE

Department of Physical and Macromolecular Chemistry

INSTITUTE OF MACROMOLECULAR CHEMISTRY
AS CR, v.v.i.
Department of Supramolecular Polymer Systems

Aliphatic polyester-based nanoparticles as drug delivery systems

Doctoral thesis

MSc Alessandro Jäger

Supervisor: RNDr. Petr Štěpánek, DrSc.

PRAGUE 2015

Přírodovědecká fakulta
UNIVERZITY KARLOVY V PRAZE

Katedra fyzikální a makromolekulární chemie

ÚSTAV MAKROMOLEKULÁRNÍ CHEMIE AV ČR, v.v.i.

Oddělení nadmolekulární polymerní systémy

Alifatické nanočástice polyester na bázi například systémy podávání léků

Dizertační práce

Mgr. Alessandro Jäger

Školitel: RNDr. Petr Štěpánek, DrSc.

PRAHA 2015

Prohlášení:

Prohlašuji, že jsem předkládanou závěrečnou práci zpracoval sám a že jsem uvedl všechny použité informační zdroje a literaturu. Předkládaná práce ani její část nebyla předložena k získání jiného nebo stejného akademického titulu.

Declaration:

Hereby I declare that I have worked out this doctoral thesis independently, under the guidance of RNDr. Petr Štěpánek, DrSc. and I have fully cited all sources used. This work has not been used in order to gain any other academic degree.

Prague 18.5.2015

Signature

Acknowledgement

First of all, I would like to express my thankfulness to my supervisor RNDr. Petr Štěpánek, DrSc. for the great opportunity and honor of his advice, support, and motivation with my work.
My special thanks belong to my brother MSc. Eliezer Jäger for his immensurable help with fruitful discussions, compromise and dedication to the field of drug delivery. As brothers science was able to make us closer friends.
I also would like to thanks all my colleagues of department, where this work was done, for always try to keep the mood at the highest levels during work and out of it.

And finally a special grateful to my wife, who always was a lovely partner since 2010, patient and dedicated to me, and to my parents who are my personal inspiration.

Abstract

Nanoparticles from biodegradable polymers are considered one of the most promising systems for biomedical application as drug delivery systems. Therefore, the synthesis and characterization of a new aliphatic biodegradable copolyester named PBS/PBDL (poly(butylene succinate-*co*-butylene dilinoleate)) intended to the application as drug delivery system is reported in the thesis. Surfactant-free biodegradable and narrowly distributed, nanosized spherical particles (R_H < 60 nm) have been produced from the biodegradable material by applying a single-step nanoprecipitation protocol. The size of the generated polymer nanoparticles (PNPs) could be controlled by adjusting the polymer concentration, the choice of organic solvent, mixing different organic solvents or by changing temperature and ionic strength. By optimizing such parameters sub-100 nm uniform PNPs can be produced through this methodology including the advantage and ability to scale-up production. The nanoparticles structure was characterized in detail by employing a variety of scattering techniques and transmission electron microscopy (TEM). Combined static light scattering (SLS) and dynamic light scattering (DLS) measurements suggested that the nanoparticles comprise a porous core conferring them a non-compact characteristic. Their porosity enables water to be entrapped which is responsible for their pronounced stability and relatively fast degradation as followed by size exclusion chromatography (SEC). The polymeric nanoparticles could be loaded with the hydrophobic antitumoral drug paclitaxel (PTX) and doxorubicin (DOX) with a drug loading content of ~ 6–7% $w_{drug}/w_{polymer}$ and ~ 5% $w_{drug}/w_{polymer}$, respectively. The drug encapsulation and release modifies the inner structure of the nanoparticles, which holds a large amount of entrapped water in the drug-free condition. The controlled DOX release is pH-dependent and faster under slightly acidic conditions and the cell viability experiments demonstrated that the drug-free NPs are non-toxic, whereas the DOX-loaded NPs exert *in vitro* cytostatic efficacy on EL4 T cell lymphoma. Finally, the successful coverage of the hydrophobic PBS/PBDL NPs by the non-immunogenic and non-toxic hydrophilic *N*-(2- hydroxypropyl)methacrylamide (HPMA) copolymer makes them an alternative to the biodegradable FDA-approved polyester and PEG-shielded nanoparticles for biomedical application as drug delivery systems.

Keywords: paclitaxel, doxorubicin, biodegradable polyester, drug delivery systems, PHPMA, light scattering

Contents

List of abbreviations

AIDS	Acquired Immune Deficiency Syndrome
DLA	dilinoleic acid
DLS	dynamic light scattering
DMSO	dimethylsufoxide
DMF	dimethylformamide
DOX	doxorubicin
EPR	enhanced permeability and retention
FA	fatty acids
FDA	Food and Drug Administration
HPMA	N-(2- hydroxypropyl)methacrylamide)
[M]	organometallics
Nu	nucleophiles
PBS/PBDL	poly(butylene succinate-*co*-butylene dilinoleate)
PDI	polydispersity index
PCL	poly(*ε*-caprolactone)
PEG	polyethylene glycol
PLA	poly(*D,L*-lactic acid)
PLGA	poly(*D,L*-lactide-*co*-glycolide)
PNPs	polymer nanoparticles
PTX	paclitaxel
ROP	ring opening polymerization
SA	succinic acid
SEC	size exclusion chromatography
SLS	static light scattering
TCA	tricarboxylic acid cycle
THF	thetrahydrofuran
TEM	transmission electron microscopy

List of symbols

δ_p	Scatchard-Hildebrand solubility parameter of the polymer
δ_S	Scatchard-Hildebrand solubility parameter of the solubilized drug
χ	Flory-Higgins interaction parameter
υ_s	molar volume of the solubilized drug
R	gas constant or
T	temperature (in Kelvin)
T_g	glass transition
R_H	hydrodynamic radius
R_G	radius of gyration
$\overline{X}_n$	number average degree of polymerization
$\overline{X}_w$	weight average degree of polymerization
p	degree of conversion
k_p	equilibrium constant of polycondensation
$\vec{m}$	electric dipole momentum
α	polarizability
$\vec{E}$	electric field vector
v	frequency of the light
λ	wavelength
$\vec{k}$	length of the wave vector
E_s	electrical field vector of the scatter light
$\overrightarrow{r_D}$	distance vector from the scattering sample to the detector
c	speed of light in vacuum or concentration
I_s	scattering intensity
b^2, k	single particle scattering power or contrast factor
n_D	refractive index of the solute
$n_{D,0}$	refractive index of the solvent
N_A	Avogadro number
d_n/d_c	refractive index increment
R_θ	Rayleigh ratio

M_w	weight average molar mass
M_n	number average molar mass
θ	angle
A_2	second virial coefficient
Γ	decay rate
μ_2	second cumulant
D	diffusion coefficient
η	solvent viscosity
k_B	Boltzmann constant
$P(q)$	form factor
$S(q)$	structure factor
d	density of nanoparticles
$\overline{D_N}$	number average diameter
$\overline{D_W}$	weight average diameter
$\overline{D_Z}$	zeta average diameter
P_{TEM}	transmission electron microscopy polydispersity index

1.1 Introduction

Biomedical application of nanomaterials has emerged as one of the most significant trends in the area of nanotechnology.[1,2,3] The research interest in the field has recently transferred from semiconductor chips to biomedical applications. Polymeric nanomaterials for biomedical applications are of research interest since the early 1990s.[4] The nanometer size of polymeric nanoparticles, which is much smaller than that of blood cells, could readily move in biological environments (Figure 1.1). Encapsulation of drugs and imaging agents into polymeric nanoparticles through physical or chemical conjugation was found to have great potential in drug delivery and diagnostic applications. Polymer-based nanoparticles are the most extensively studied nano-sized drug carriers.[5,6,7,8,9,10,11,12] Commonly, the present nanoparticles used for drug delivery have a size ranging between 1 nm and 1000 nm and characterized by versatile structures and morphologies.[13]

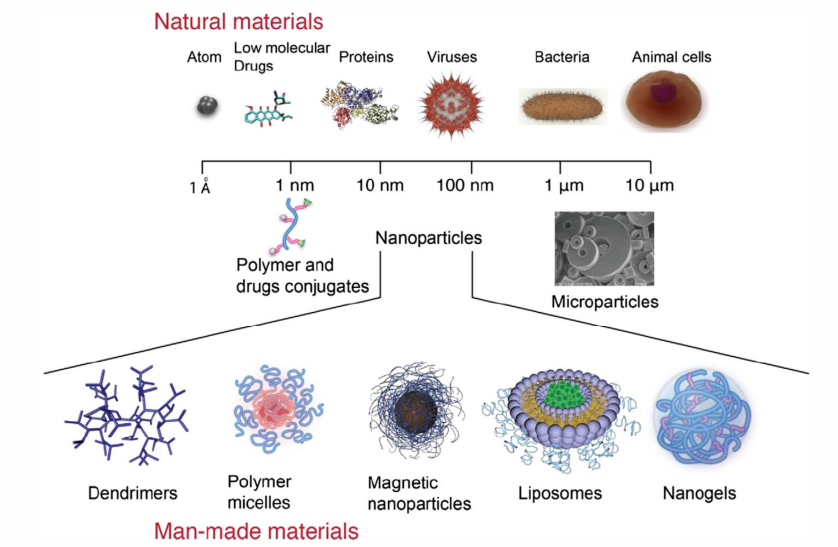

Figure 1.1. Schematic example of size comparison between the man-made nanoparticles intended to drug delivery applications and the biological systems.[14]

Nanoparticles from biodegradable polymers are considered one of the most promising systems for biomedical application as drug delivery systems[7,15,16,17] Some examples of their versatility include; (1) the ability to cross the biological barriers to reach the target sites and enter the cells due to their small sizes, thus achieving an improved therapeutic effect; (2) the capability for protecting the drug from degradation and for sustained release of the therapeutic

drug in specific sites; (3) the tenability of the drug release through modulating both drug diffusion in nanoparticles and polymer degradation; (4) the possibility of polymer modification, which incorporates targeting ligands and biological active components onto the surface of the nanoparticles; (5) and the easy elimination of the drug carriers from the body after polymer degradation.

1.2 Biodegradable polymer nanoparticles

As mentioned above, biodegradable nanoparticles have been intensely used as drug delivery vehicles due to their good properties such as bioavailability, better encapsulation, control release and lower toxicity.[18] Various biodegradable nanoparticulate systems were reported in the literature describing the encapsulation process, controlled release and improvement of therapeutic value of nanoencapsulated drugs. Some examples of biodegradable nanomedicines for treatment of diseases like cancer[19], diabetes[20], AIDS[21], malaria[22] and tuberculosis[23] are in different trial phases for testing and some of them are already commercially available.[24,25,26]

The most extensively studied biodegradable polymer nanoparticles are those based on Food and Drug Administration (FDA) approved polymers. Some examples of the most commonly applied biodegradable polymer nanoparticles are poly(D,L-lactide-*co*-glycolide) (PLGA), poly(D,L-lactic acid) (PLA), poly(ε-caprolactone) (PCL), poly(alkyl cyanoacrylates), chitosan and gelatin.[4,8,27,28,29] Shortly, a few examples related to their drug encapsulation and therapeutic advantages are given.

1.2.1 PLGA nanoparticles

Until today, PLGA is one of the most successfully used biodegradable nanoparticulate system manly because it undergoes hydrolysis in the body producing nontoxic metabolite monomers, lactic acid and glycolic acid.[18] PLGA nanoparticles have been used in the development of several therapeutic nanosystems like cancer, immune diseases, inflammation, diabetes, schizophrenia and others.[7,8,30,31] However, the effectiveness of anti-cancer agents such as paclitaxel,[32,33,34] doxorubicin[35,36,37] and cisplatin[38,39,40] using PLGA nanoparticles were by far the most studies drug delivery systems in the literature. Although the performance of these nanoparticles is not completely satisfactory, the relative success of these loaded nanocarriers is associated to their ability to protect poorly soluble and unstable payloads from the biological milieu and to be small enough for capillary penetrations, cellular internalization

and endosomal escape.[34,41] Furthermore, PLGA-based nanoparticles can increase the efficacy of treatments because of the sustained release of the therapeutic agent from stable nanoparticles which improves the pharmacokinetic and pharmacodynamic profiles.[19,26,32,42] Therefore in comparison to the others non-biodegradable systems, PLGA-based nanoparticles are always in a good position for clinical trials.[30]

1.2.2 PLA nanoparticles

Unmistakably, PLA nanoparticles are one of the most studied biodegradable nanosystems for drug release applications in the general therapy.[43] In the body, PLA-based nanoparticles are biodegraded to monomeric units of lactic acid which is a natural intermediate by-product of anaerobic respiration, later converted into glucose by the liver during the Cori cycle.[44] In comparison to PLGA, the PLA nanoparticles are more hydrophobic and have a slower degradation rate.[45,46] Nevertheless, in general they are able to load higher amounts of hydrophobic drug in comparison to PLGA nanoparticles.[47,48] Similarly to PLGA, the PLA-based nanoparticles were used for encapsulate psychotic drugs,[49] hormones,[50] proteins,[51] anti-cancer[26,52] and anti-inflammatory[53] agents, and others.[8,31,54] The therapeutic improvement of the drug loaded PLA-based nanoparticles is related mainly to the sustained release, prolonged blood circulation time, enhanced cell uptake and bioavailability.[26,53,55,56,57] These above mentioned therapeutic benefits of PLA-based nanoparticles make them promising tools for drug release application in the therapy of several diseases. Together with PLGA, the PLA-based nanoparticles are a reality in the current clinical application and in the market.[26,5859]

1.2.3 PCL nanoparticles

In comparison to the amorphous PLGA and PLA, nanoparticles produced from the semicrystalline PCL are the most hydrophobic, therefore their polymer matrix have the slowest degradation rate allowing drug release up to several months.[60,61] Although the PLC-based nanoparticles were extensively studied in the encapsulation of anticancer,[62,63,64] anti-diabetes,[65] antidepressive,[66,67] antifungical agents,[68] etc, the main application in the therapy is related to their long term sustained release of loaded drugs.[60,61,69,70] Therefore, the application as injectable nanocarries in the therapy is limited mainly because of the slow degradation rates of the PCL-based nanoparticles in comparison to PLGA and PLA.

1.3 Drug loading in biodegradable nanoparticles

A successful nanoparticle system is characterized by a high loading capacity which reduces the quantity of the carrier required for administration.[4,27] Higher drug loadings into nanoparticles are achieved by incorporating the drug at the time of nanoparticle production.[71] In general, the drug is dissolved with the polymer in a common solvent and the resulted solution is exchanged against a bad solvent for both components.[72] In general, the result is the encapsulation of the drug in the polymer matrix which can be physically dissolved or dispersed.[73]

When discussing drug loading into the polymer matrix, it is assumed that the two components are mixed homogeneously at the molecular level.[74] This important assumption is directly related to the solubility (for the crystalline host molecules) and/or miscibility (for the amorphous load) of the polymer matrix. The solubility is defined by the thermodynamic equilibrium parameter δ, at which the chemical potential of the solute in the solid phase is the same as that in the liquid (solution) phase.[75,76] In general, the miscibility of a small drug molecule in a polymer matrix is a complex equilibrium, since the amorphous drug is usually meta-stable in comparison to the crystalline state and shows an inclination to crystallize.[744]

The lattice-based Flory–Huggins theory of polymer solutions proposes an expression for the calculation of overall free energy of dissolution per mole of lattice site and has been successfully applied to predict the behavior of polymer-solvent systems. It is expected that the degree of dissolution will increase when the value of the Flory-Huggins interaction parameter (χ_{dp}) decreases. The greatest degree of solubilization occurs when high compatibility exists between the polymer matrix and the drug, according to

$$\chi_{dp} = \frac{(\delta_d - \delta_p)^2 \upsilon_d}{RT} \qquad (1)$$

where δ_d and δ_p are the Scatchard-Hildebrand solubility parameters of the drug and the polymer, respectively, υ_p is the molar volume of the solubilized drug, R is the gas constant and T the Kelvin temperature. As noticed, the highest compatibility is achieved when δ_d and δ_p are every close.

Although the lack of studies focused on the influence of polymer crystallinity, glass transition (Tg) and morphology on the drug loading of nanoparticles makes difficult to have conclusive assumptions, the evaluation of the mentioned parameters should not be neglected.

In some cases, a reduction in the loading of drug in the nanoparticles was observed with the increase of the polymer crystallinity and T*g*, whereas in others no significant changes could be observed.[77,78,79,80] Furthermore, several studies demonstrates that the drug loading capacity of the nanoparticles can be significantly enhanced only when the hydrophobic effect between the polymer and drugs is combined with hydrogen bonding, electrostatic interaction and dipole–dipole interactions.[81,82,83,84]

Other crucial parameter involved in the efficiency of the drug entrapped in the nanoparticles is the preparation technique.[71] Since our studies are focused on the solvent displacement technique (nanoprecipitation), the highest entrapment efficiency is reached at the lowest molecule solubility in the aqueous phase, the fastest rate of polymer precipitation, the largest amorphous-state solubility of the molecule in the polymer and the highest affinity between the organic solvents and the aqueous phase.[71,733,85]

1.4 General methods of preparation of biodegradable nanoparticles

Nowadays, several methods for preparing submicron particles from preformed polymers are available.[711,86] They can be divided into two groups depending on the steps involved in their preparation.[87] Examples of the first group are emulsification-diffusion (also called emulsification-solvent displacement), emulsification-evaporation and emulsification-coacervation. In general they are based on two steps, in which the first is characterized by preparation of an emulsion while the second is based on particle formation by polymer precipitation or cross-linking. The second group of methods does not require the emulsion preparation step in order to obtaining the particles. The nanoparticles preparation is based on polymer precipitation under conditions of spontaneous dispersion.[88] Therefore, in this case the particles are formed from a polymer solution or the self-assembly of macromolecules, or the synthesis of polyelectrolyte complexes. One example of the most extensively applied procedure of this type is the solvent displacement (also termed nanoprecipitation, solvent diffusion or interfacial deposition).[86,87,88,89]

1.4.1 Solvent displacement technique (nanoprecipitation)

As mentioned above, the nanoprecipitation is a representative example of one of the most commonly used techniques for the preparation of polymer nanoparticles for biomedical applications. It is characterized by procedural simplicity, high encapsulation efficiency, high reproducibility, low possible contaminant content (eg. low amounts of stabilizing agents), low

cost and easy up-scaling.[88,89,88,90,91,92] Furthermore, it uses preformed polymers as starting materials rather than monomers and toxic solvents which makes clinical translation much easier.[93,94]

Since the production of nanoparticles by solvent nanoprecipitation technique is characterized by a low-energy mixing process based on self-diffusion, it requires miscibility between the solvent and nonsolvent phases.[95] The solvent phase consists of a solution of the drug and the polymer. The nonsolvent phase is composed by nonsolvent or a mixture of nonsolvents for the polymer, which can be supplemented or not with one or more surfactants.[71,88,89] In general, solvent and nonsolvent phases are called organic and aqueous phases, respectively, because the solvent is an organic medium while water is mainly the nonsolvent. One example of polymer nanoparticles preparation by nanoprecipitation is given in figure 1.2. The organic phase is mixed with the stirred aqueous phase in one shot, stepwise, dropwise or by controlled addition rate.[96] The polymer nanoparticles are formed instantaneously and the solvent is removed from the system by using evaporation under reduced pressure.

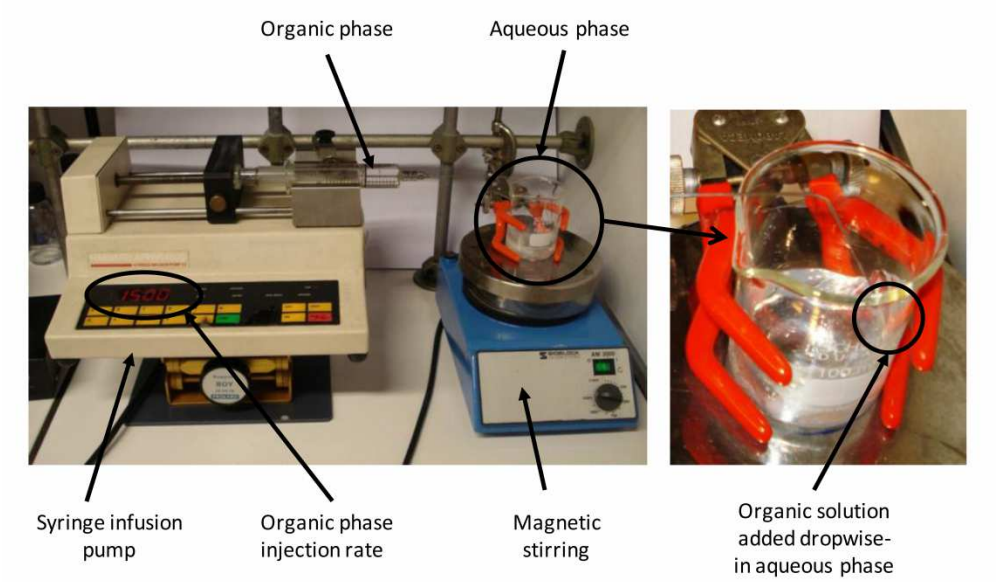

Fig. 1.2. Laboratory set-up for preparing polymer nanoparticles by nanoprecipiation.

The operating conditions involved in the nanoprecitation technique are shown in Figure 1.3.

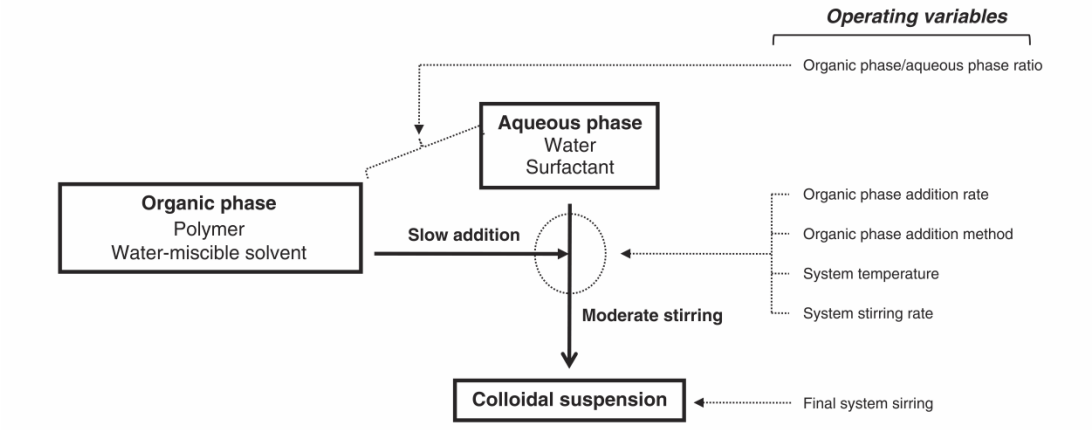

Figure 1.3. Schematic procedure and operating variables involved in the nanoprecipitation technique.

The influence of some of these parameters such as phase mixing method, the organic phase addition rate, the organic/aqueous phase ratio, stirring rate and temperature on the final size distribution of the nanoparticles were extensively studied.[71,87,88,89,96] However, as will be discussed along the thesis, the mechanics involved in the particles formation by nanoprecipitation is still an open debate. Therefore, studies related to the physicochemical parameters involved in the nanoprecipitation technique are essential for the biomedical applications.

1.5 References

[1] Y. Xia, *Nat. Mater.*, **2008**, 7, 758 – 760.

[2] C. Lok, *Nature*, **2010**, 467, 18-21.

[3] R. Juliano, *Nature Reviews Drug Discovery*, **2013**, 12, 171-172.

[4] K. E. Uhrich, S. M Cannizzaro, R. S. Langer, K. M. Shakesheff, *Chem. Rev.*, **1999**, *99*, 3181-3198.

[5] C. Allen, D. Maysinger, A. Eisenberg, *Colloid. Surface B*, 1999, 16, 3-27.

[6] A. Rösler, G. W. M. Vandermeulen, H.-A. Klok, *Adv. Drug Deliver. Rev.*, **2001**, *53*, 95–108.

[7] K. A. Woodrow, Y. Cu, C. J. Booth, J. K. Saucier-Sawyer, M. J. Wood, W. M. Saltzman, *Nat. Mater.*, **2009**, *8*, 526 – 533.

[8] A. Kumari, S. K. Yadav, S. C. Yadav, *Colloid. Surface B*, 2010, 75, 1-18.

[9] J. Shi, Z. Xiao, N. Kamaly, O. C. Farokhzad, *Accounts Chem. Res.*, **2011**, *44*, 1123–1134.

[10] R. Duncan, R. Gaspar, *Mol. Pharmaceutics*, **2011**, *8*, 2101-2141.

[11] M. L. Etheridge, S. A. Campbell, A. G. Erdman, C. L. Haynes, S. M. Wolf, J. McCullough, *Nanomed-Nanotechnol*, **2013**, *9*, 1-14.

[12] R. Duncan, *J. Control. Release*, **2014**, *190*, 371-380.

[13] European Union Scientific Committee on Emerging and Newly Identified Health Risks. Scientific Basis for the Definition of the Term “nanomaterial”; 2010; ISSN 1831 4783 ISBN 978-92-79-12757-1; doi:10.2772/39703 ND-AS-09-004-EN-N.

[14] Y. Zhao, D. Y. Alakhova, A. V. Kabanov, *Adv. Drug Deliver. Rev.*, **2013**, *65*, 1763–1783.

[15] M. Eaton, *Nat. Mater.*, **2007**, *6*, 251-253.

[16] N. Rapoport, *Prog. Polym. Sci.*, **2007**, *32*, 962–990.

[17] S. Mitragotri, J. Lahann, *Nat. Mater.*, **2009**, *8*, 15–23.

[18] B. Semete, L. Booysen, Y. Lemmer, L. Kalombo, L. Katata, J. Verschoor, H. S. Swai, *Nanomed. Nanotechnol. Biol.*, **2010**, *6*, 662–671.

[19] L. Mu, S. S. Feng, *J. Control. Release*, **2003**, *86*, 33–48.

[20] C. Damge, P. Maincent, N. Ubrich, *J. Control. Release*, **2007**, *117*, 163–170.

[21] C. Coester, J. Kreuter, H. von Briesen H, K. Langer , *Int. J. Pharm.*, **2000**, *196*, 147–149.

[22] A. A. Date, M. D. Joshi, V. B. Patravale, *Adv. Drug Deliv. Rev.*, **2007**, *59*, 505–521.

[23] I. P. Kaur, H Singh, *J. Control. Release*, **2014**, *184*, 36–50.

[24] D. Peer, J. M. Karp, S Hong, O. C. Farokhzad, R. Margalit, R. Langer, *Nat. Nanotechnol.*, **2007**, *2*, 751-760.

[25] K. S. Lee, H C. Chung, S A Im, Y H Park, C. S Kim, S.-B. Kim, S. Y. Rha, M. Y. Lee, J. Ro, *Breast Cancer Res. Treat.*, **2008**, *108*, 241–250.

[26] J. Hrkach, D. V. Hoff, M. M. Ali, E. Andrianova, J. Auer, T. Campbell, D. D. Witt, M. Figa, M. Figueiredo, A. Horhota, S. Low, K. McDonnell, E. Peeke, B. Retnarajan, A. Sabnis, E. Schnipper, J. J. Song, Y. H. Song, J. Summa, D. Tompsett, G. Troiano, T. V. G. Hoven, J. Wright, P. LoRusso, P. W. Kantoff, N. H. Bander, C. Sweeney, O. C. Farokhzad, R. Langer, S. Zale, *Sci. Transl. Med.*, **2012**, 1-11.

[27] K. S. Soppimath, T. M. Aminabhavi, A. R. Kulkarni, W. E. Rudzinski, *J. Control. Release*, **2001**, *70*, 1–20.

[28] M. L. Hans, A. M. Lowman, *Curr. Opin. Solid St Mat.*, **2002**, *6*, 319-327.

[29] J. Panyam, V. Labhasetwar, *Adv. Drug Deliv. Rev.*, **2003**, *55*, 329–347.

[30] F. Danhier, E. Ansorena, J. M. Silva, R. Coco, A. Le Breton, V. Préat, *J. Control. Release*, **2012**, *161*, 505–522.

[31] J. Li, C, Sabliov, *Nanotechnol. Rev.*, **2013**, *2*, 241–257.

[32] C. Fonseca, S. Simoes, R. Gaspar, *J. Control. Release*, **2002**, *83*, 273–286.

[33] L. Mu, S.S. Feng, *J. Control. Release*, **2003**, *86*, 33–48.

[34] F. Danhier, N. Lecouturier, B. Vroman, C. Jerome, J. Marchand-Brynaert, O. Feron, V. Preat, *J. Control. Release*, **2009**, *133*, 11–17.

[35] T. Betancourt, B. Brown, L. Brannon-Peppas, *Nanomedicine*, **2007**, *2*, 219-232.

[36] C. Chittasupho, S.X. Xie, A. Baoum, T. Yakovleva, T.J. Siahaan, C.J. Berkland, *Eur. J. Pharm. Sci.*, **2009**, *37*, 141–150.

[37] I. Amjadi, M. Rabiee, M. S. Hosseini, M. Mozafari, *Appl. Biochem. Biotechnol.*, **2012**, *168*, 1434–1447.

[38] K. Avgoustakis, A. Beletsi, Z. Panagi, P. Klepetsanis, A. G. Karydas, D. S. Ithakissios, *J. Control. Release*, **2002**, *79*, 123–135.

[39] S. Dhar, F. X. Gu, R. Langer, O. C. Farokhzad, S. J. Lippard, Proc. Natl. Acad. Sci. U. S. A., **2008**, *105*, 17356–17361.

[40] C. Menale, M T. Piccolo, I. Favicchia, M G. Aruta, A. Baldi, C. Nicolucci, V. Barba, D. G. Mita, S. Crispi, N. Diano, *Pharm. Res.*, **2015**, *32*, 362-374.

[41] J. Panyam, W.-Z. Zhou, S. Prabha, S. K. Sahoo, V. Labhasetwar, *FASEB J.*, **2002**, *16*, 1217–1226.

[42] L. Zhao, S.-S. Feng, *J. Pharm. Sci.*, **2010**, *99*, 3552-3560.

[43] V. Lassalle, M. L. Ferreira, *Macromol. Biosci.*, **2007**, *7*, 767–783.

[44] A. Mahapatro, D. K. Singh, *J. Nanobiotechnology*, **2011**, 9:55.

[45] J. M. Anderson, M. S. Shive, *Adv. Drug Deliv. Rev.*, **1997**, *28*, 5–24.

[46] M. L.T. Zweers, G. H. M. Engbers, D. W. Grijpma, J. Feijen, J. Control. Release, 2004, 100, 347-356.

[47] T. Musumeci, C. A. Ventura, I. Giannone, B. Ruozi, L. Montenegro, R. Pignatello, G. Puglisi, *Int. J. Pharm.*, **2006**, *325*, 172-179.

[48] S. Islam, *Int. J. Pharm. Pharm. Sci*, **2011**, *3*, 181-188.

[49] J-C Leroux, E. Allémann, F. D. Jaeghere, E. Doelker, R. Gurny, *J. Control. Release*, **1996**, *39*, 339.

[50] J. Matsumoto, Y. Nakada, K. Sakurai, T. Nakamura, Y. Takahashi, *Int. J. Pharm.*, **1999**, *185*, 93–101.

[51] H. Gao, Y. N. Wang, Y. G. Fan, J. B. Ma, *J. Control. Release*, **2005**, *107*, 158–173.

[52] J. Xing, D. Zhang, T. Tan, *Int. J. Biol. Macromol.*, **2007**, *2*, 153–158.

[53] C. Gomez-Gaete, E. Fattal, L. Silva, M. Besnard, N. Tsapis, *J. Control. Release*, **2008**, *128*, 41–49.

[54] I. Fishbein, M. Chorny, L. Rabinovich, S. Banai, I. Gati, G. Golomb, *J. Control. Release*, **2000**, *65*, 221–229.

[55] A. Budhian, S. J. Siegel, K. I. Winey, *J. Microencapsul.*, **2005**, *22*, 773–785.

[56] D. K. Sahana, G. Mittal, V. Bhardwaj, M. N. Kumar, *J. Pharm. Sci.*, **2008**, *97*, 1530–1542.

[57] S. H. Lee, Z. Zhang, S. S. Feng, *Biomaterials*, **2007**, *28*, 2041–2050.

[58] N. Kamaly, Z. Xiao, P. M. Valencia, A. F. Radovic-Moreno, O. C. Farokhzada, *Chem. Soc. Rev.*, **2012**, 41, 2971–3010.

[59] S.-W. Lee, M.-H. Yun, S. W. Jeong, C.-H. In, J-Y. Kim, M.-H. Seo, C-M Pai, S-O Kim, *J. Control. Release*, **2011**, *155*, 262–271.

[60] V. R. Sinha, K. Bansal, R. Kaushik, R. Kumria, A. Trehan, *Int. J. Pharm.*, **2004**, *278*, 1–23.

[61] L. S. Naira, C. T. Laurencin, *Prog. Polym. Sci.*, **2007**, *32*, 762–798.

[62] D. Zheng, X. Li, H. Xu, X. Lu, Y. Hu, W. Fan, *Acta Biochim. Biophys. Sin.*, **2009**, *41*, 578–587.

[63] S. Y. Kim, Y. M. Lee, *Biomaterials*, **2001**, *22*, 1697–1704.

[64] D. B. Shenoy, M. M. Amiji, *Int. J. Pharm.*, **2005**, *293*, 261–270.

[65] C. Damge, P. Maincent, N. Ubrich, *J. Control. Release*, **2007**, *117*, 163–170.

[66] M. L.-L. Verger, L. Fluckiger, Y. I. Kim, M. Hoffman, P. Maincent, *Eur. J. Pharm. Biopharm.* 1998, 46, 137–143.

[67] C. Changyong, S. Y. Chae, N. Jae-Won, *Polymer*, **2006**, *47*, 4571-4580.

[68] M. S. Espuelas, P. Legrand, P. M. Loiseau, C. Bories, G. Barratt, J. M. Irache, *J. Drug Target*, **2002**, *10*, 593–599.

[69] V. Tamboli, G. P. Mishra, A. K. Mitra, *Colloid Polym. Sci.*, **2013**, *291*, 1235-1245.

[70] U. Bazylińskaa, A. Lewińskab, Ł. Lamcha, K. A. Wilka, *Colloid. Surface A*, **2014**, 442, 42-49.

[71] C. E. Mora-Huertas, H. Fessi, A. Elaissari, *Adv. Colloid Interfac.*, **2011**, 163, 90-122.

[72] J. G. J. L. Lebouillea, R. Stepanyanb, J. J. M. Slotb, M. A. Cohen Stuartd, R. Tuiniera, *Colloid. Surface A*, **2014**, 460, 225-235.

[73] J. V. Natarajan, C. Nugraha, X. W. Ng, S. Venkatraman, *J. Control. Release*, **2014**, *193*, 122–138.

[74] A. Kowalczuka, R. Trzcinskaa, B. Trzebickaa, A. H. E. Müller, A. Dworaka, C. B. Tsvetanovc, *Prog. Polym. Sci.*, **2014**, *39*, 43–86.

[75] J. H. Hildebrand, *Chem. Rev.*, **1949**, *44*, 37-45.

[76] C. M. Hansen, *J. Paint Technol.*, **1967**, *39*, 104-17.

[77] H. Ge, Y. Hu, S. Yang, X. Jiang, C. Yang, J. *Appl. Polym. Sci.*, **2000**, **75**, 874-882.

[78] Q. Liu, C. Cai, C.-M. Dong, *J. Biomed. Mater. Res. A*, **2009**, *88*, 990-999.

[79] V. Karavelidis, E. Karavas, D. Giliopoulos, S. Papadimitriou, D. Bikiaris, *Int. J. Nanomed.*, **2011**, *6*, 3021–3032.

[80] D. Bikiaris, V. Karavelidis, E. Karavas, *Molecules*, **2009**, *14*, 2410-2430.

[81] A. Lavasanifar, J. Samuel, S. Sattari, G. S. Kwon, *Pharm. Res.*, **2002**, *19*, 418-422.

[82] K. M. Huh, H. S. Min, S. C. Lee, H. J. Lee, S. Kim, K. Park, *J. Control. Release*, **2008**, *126*, 122-129.

[83] A. Mahmud, S. Patel, O. Molavi, P. Choi, J. Samuel, A. Lavasanifar, *Biomacromolecules*, **2009**, *10*, 471–478.

[84] S. K. Patel, A. Lavasanifar, P. Choi, *Biomacromolecules*, **2009**,*10*, 2584-2591.

[85] D. K. Sahana, G. Mittal, V. Bhardwaj, M. N. Kumar, *J. Pharm. Sci.*, **2008**, *97*, 1530-1542.

[86] C. P. Reis, R. J. Neufeld, A. J. Ribeiro, F. Veiga, *Nanomed-Nanotechnol.*, **2006**, 8– 21.

[87] Vauthier C, Bouchemal K. *Pharm. Res.*, **2009**, *26*, 1025-1058.

[88] E. Lepeltier, C. Bourgaux, P. Couvreur, *Adv. Drug Deliv. Rev.*, **2014**, *71*, 86-97.

[89] C. E. Mora, H. Fessi, A. Elaissari, *Int. J. Pharm.*, **2010**, *385*, 113-142.

[90] M. Chorny, I. Fishbein, H. D. Danenberg, G. Golomb, *J. Control. Release*, **2002**, *83*,389-400.

[91] E. Cauchetier, M. Deniau, H. Fessi, A. Astier, M. Paul, *Int J Pharm*, **2003**, *250*, 273.

[92] A. Budhian, S. J. Siegel, K. I. Winey, *Int. J. Pharm.*, **2007**, *336*, 367-375.

[93] D. Moinard, Y. Chevalier, S. Briançon, H. Fessi, S. Guinebretière, *J. Nanosci. Nanotechnol.*, **2006**, *6*, 2664.

[94] H. Fessi, F. Puisieux, J. P. Devissaguet, N. Ammoury, S. Benita, Int. J. Pharm., **1989**, *55*, R1.

[95] S. A. Vitale, J. L. Katz, *Langmuir*, **2003**,*19*, 4105-4110.

[96] E. Sah, H. Sah, Journal of Nanomaterials, 2015, *J. Nanomater.*, **2015**, 794601.

2.1 Goals of the Thesis

The main objective of my Thesis is to prepare aliphatic polyester-based nanoparticles for drug delivery applications. Taking into account the significance of the application strict request such as biocompatibility, biodegradability, controlled size distribution and drug release are basic concepts which must be fulfilled. Therefore, the work was divided into chapters which contain the background with the detailed description of each particular goal and the resulting achievements. The specific goals are listed below:

- Synthesis and characterization of poly(butylene succinate-*co*-butylene dilinoleate (PBS/PBDL) copolyester as an alternative to FDA approved polyesters.
- Evaluation of the influence of the physicochemical parameters (eg. polymer concentration, solvent nature and ratio, etc) on the particle size distribution of the polyester nanoparticles prepared by nanoprecipitation technique.
- Loading the polyester nanoparticles using the hydrophobic paclitaxel as drug model
- Loading the PHPMA covered PBS/PBDL copolyester nanoparticles with doxorubicin and tests its *in vitro* cytotoxicity on cancer cells.

3. General synthetic approaches and characterization

3.1 Introduction

This chapter describes the general methods utilized in this thesis for the preparation and characterization of the polymers and the nanoparticles studied as well as the reasons behind the selection of the applied methodology. Due to the comprehensive description of synthetic and characterization methodologies in the publications attached, the following chapter only aims at introducing the reader to the main synthetic concepts behind polymer design and nanoparticles preparation. Precise description of the methodologies of synthesis, characterization and preparation can be found in the Appendices attached.

3.2 Synthesis of the aliphatic polyesters

Aliphatic polyesters constitute one of the most important classes of synthetic biodegradable and biocompatible polymer intended for biomedical applications.[1,2,3] They are commercially available in several types. Some examples of FDA-approved aliphatic polyesters mentioned in the thesis are polycaprolactone (PCL)[4,5], poly(L-lactide) (PLA)[6,7] and poly(lactic-co-glycolic acid) (PLGA)[8]. They have been extensively studied for their biocompatibility[9,10,11,12], biodegradability[13,14] and bioresorbability[15]. It was found that they are highly biocompatible materials[16], easily hydrolysable into human body[17,18,19] and therefore they can be used for biomedical applications in the production of drug carrier devices for controlled release[20,21,22,23]. Among the FDA-approved polymers, polybutylene succinate (PBS) is also an important commercially available biodegradable aliphatic polyester derived from fatty C-4 compounds.[24,25,26,27] The absence of cytotoxic degradation products, [e.g. succinic acid is an intermediate in the TCA cycle (tricarboxylic acid cycle, citric acid cycle)] makes PBS copolyesters prospective candidates aiming at the development of drug delivery structures.[28,29,30,31] Furthermore, the fatty acids (FA) such as dilinoleic acid (DLA) are suitable components for the preparation of biodegradable polymers since they are hydrophobic naturally occurring body compounds[32,33] and they are able to bind encapsulated hydrophobic drugs via hydrophobic interactions when used as drug nanocarriers.[34,35,36,37]

According to Albertsson and Varma[38] the three major routes for the synthesis of aliphatic polyesters are polycondensation, ring opening polymerization (ROP) and enzymatic polymerization. Polycondensation consist of a stepwise polymerization of difunctional monomers of the AB type, ie. hydroxyl acids, or of a combination of AA and BB difunctioanl monomers resulting in the formation of a small byproduct, e. g. water.[39,40] In general, polycondensation of difunctional monomers includes the esterification of diols and diacids,

diols and diacid chlorides or the ester interchange reaction of diols and diesters (Figure 3.1).[35,36,39,41]

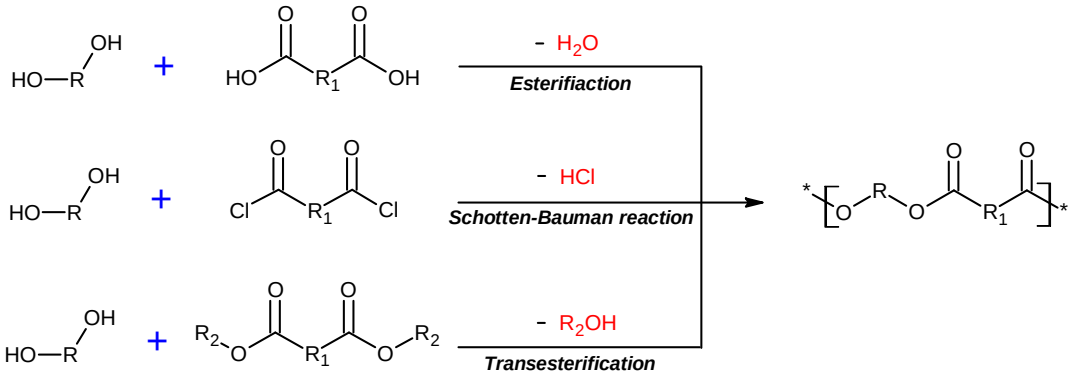

Figure 3.1. Polyester preparation by stepwise polycondensation.

Carothers published pioneering studies on polycondensation in the 1930s[42,43], and provided the fundamental analysis of step polymerization kinetics. His equation shows that high molecular weight polymers (average polymerization degree, $\overline{X}_n$ > 50) can only be achieved at very high degree of conversions (p > 98-99%)

$$\overline{X}_n = \frac{1}{1-p} \qquad (3.1)$$

Likewise in the polymerization of PBS/PBDL[35,36,37], the ester formation is characterized by an equilibrium reaction (Fig 3.2) and at least two major prerequisites must be fulfilled in order to prepare high molecular weight polymers[44,45]. First the equilibrium constant of polycondensation (K_p) has to be high enough, and the second condition is that according to equation (3.2) the stoichiometry (1:1) must be strictly obeyed in case of heteropolycondensation (eg. dialcohols and dicarboxylic acids).

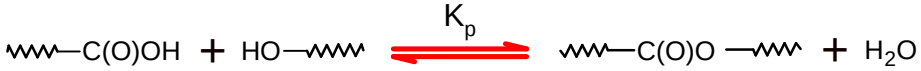

Figure 3.2. Condensation equilibrium reaction of carboxylic acids with alcohols.

In this case the number average degree of polymerization ($\overline{X}_n$) is related to K_p through the derivation of equation (3.2) and for condensation reaction of aliphatic alcohols with carboxylic acids K_p values around 10 were generally found.[40]

$$K_p = \frac{[-C(O)O-][H_2O]}{[-C(O)OH][HO-]} \quad (3.2)$$

Accordingly to equation 3.3, the resulting values of $\overline{X}_n$ around 4 for $K_p \approx$ 10 drives the polymerization reaction to the equilibrium.

$$\overline{X}_n = K_p^{0.5} + 1 \quad (3.3)$$

Since polyesters with $\overline{X}_n$ > 50 are required for fulfilling the basic physical properties of the polymer, K_p must be increased to values higher than 2400. Therefore, constant by-product removal from the reaction (eg. water and glycol)[27], high temperature settings (180-250 °C)[44,45] and the use of catalyst[46,47,48] are some of the usual strategies to drive the reaction equilibrium toward high $K_p$values resulting in higher conversion rates. However, equation (3.4) leads to one of the main drawbacks in the polycondensation, which is the increase in the polymer dispersity ($\overline{X}w/\overline{X}n$) with the increase in the conversion (p). At high conversions (p > 98-99%) the polymer dispersity $\overline{X}w/\overline{X}n$ has the tendency to approach 2.[42,49]

$$\left.\begin{aligned} \overline{X}_n &= \frac{1}{1-p} \\ \overline{X}_w &= \frac{1+p}{1-p} \end{aligned}\right\} \quad \frac{\overline{X}_n}{\overline{X}_w} = 1 + p \quad (3.4)$$

One of the options to circumvent the drawbacks from the polycondensation is using ROP polymerization of cyclic glycolide, lactides and lactones (Fig 3.3). ROP possesses several advantages compared to traditional condensation polymerization eg. mild synthetic conditions, shorter reaction times, high conversion without necessity of removal of reaction byproducts and the use of stoichiometric balance of monomers and allows good control of the polymer characteristics (predictable molecular weight and narrow molecular weight distribution).[39,41,50] All these findings make ROP the method of choice for the preparation of high-molecular weight aliphatic homo and copolyesters.

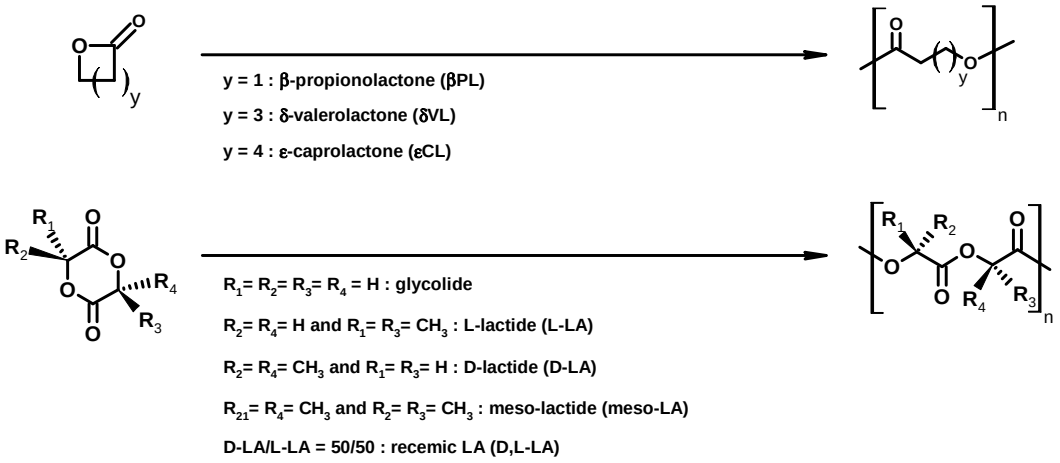

Figure 3.3. Cyclic lactides, lactones and glycolide monomers for ROP.

ROP is a flexible synthetic route where several mechanistic approaches such as anionic, cationic and coordinative initiators or catalyst have been reported.[51,52] In general, ionic (non-bulky ion pairs and free ions) are much more reactive leading to inter and intra-molecular transesterification (in case of polyester) lowering the molecular weight and broadening the molecular weight distribution of the polymer.[53] Organometallic derivatives of metals with *d*-orbitals (Al, Sn, Ti, Mg, etc) are more energetically favorable providing control to the polymerization unlike their anionic counter-part. From the several mechanisms involved in the ROP the two major ones proceed using organometallics that are acting as catalysts or as initiators. In the cases where it is used as catalyst (Fig. 3.4a) the polymerization is initiated by any nucleophile present in the polymerization medium. When it is used as initiator the polymerization proceeds through "insertion-coordination" mechanism (Fig 3.4b).

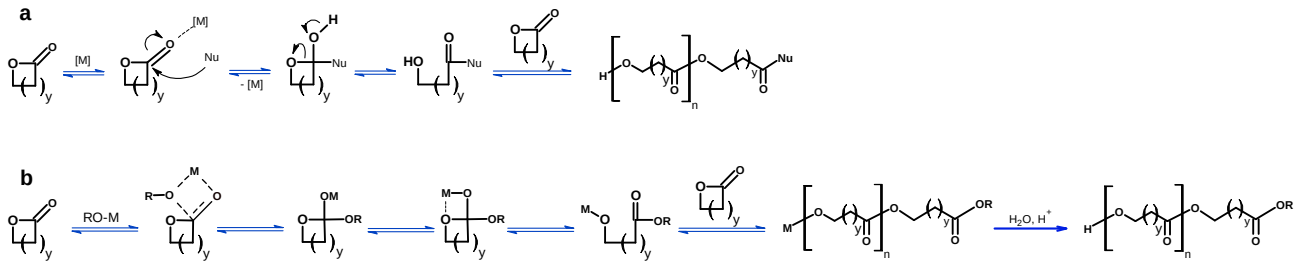

Figure 3.4. Mechanism of ROP of lactones using organometallics [M] as (a) catalyst in the presence of nucleophiles (Nu) and (b) as initiator in the "coordination-insertion" mechanism.

The third route to obtain polyester under mild conditions, avoiding the use of toxic reagents and with the possibility to recycle the catalyst is using enzymatic polymerization.

Additionally, regional and stereo selectivity of enzymes provides attractive possibilities for the direct synthesis of functional polyesters avoiding the use of protected monomers and block copolymers. However, the major drawback of the enzymatic synthesis of polyesters is the relatively low molecular weight of the obtained polymers.

3.3 Light scattering

Light scattering is one of the several phenomena resulting from the interaction between light and matter[54]. It is important to realize that all photon emission mechanisms resulting from the interaction of photons with matter arise from accelerating electrical charges. In the particular case of light scattering, when the light interacts with an isolated molecule, the oscillating electromagnetic wave induces a dipole in the molecule that oscillates with the same frequency as the incident light. What characterizes an oscillating dipole is the acceleration of charge. When a charge is accelerated, energy is emitted in all directions into a plane perpendicular to the acceleration plane. It is the energy emitted from the oscillating dipole, induced by the interaction of the incident light with the molecule, which is referred to as scattered light.[55] The frequency of the scattered light is equivalent to the oscillation frequency of the induced dipole, which is equivalent to the frequency of the incident light. Hence the frequency of the scattered light is the same as that of the incident beam and is well known as Rayleigh scattering.

For small particles and plane-polarized incident light, the scattering intensity is equal in all directions within the planes perpendicular to the polarization plane. The scattering intensity is maximum in the perpendicular plane containing the scattering center, but is zero along the axis of oscillation of the induced dipole. The scattering profile can be visualized by centering the origin on the scattering molecule with the X axis aligned with the direction of propagation of the incident light, than rotating it around the axis of oscillation. An example is given in Figure 3.5 where a small particle is illuminated by a vertically polarized incident light, the scattering angle (θ) is defined as the angle between the transmitted light axis (X) and the detector located between the XY plane. In this case, when particles are 20 times smaller than incident wavelength ($\lambda/20$), the detected scattered intensity is independent of the θ and only dependent on the mass of the particle which is proportional to the number of scattering centers contained in the particle.

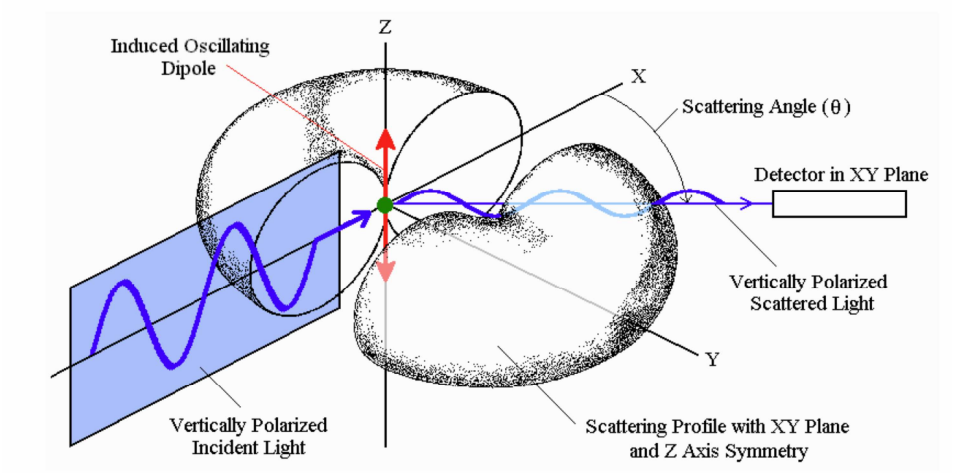

Figure 3.5. Light scattering intensity profile of small particles (reproduced from Malvern Instruments, FAQ).

When the particles are larger than 30 nm, several oscillating dipoles are generated simultaneously in the particle (Figure 3.6a). As a consequence a significant phase difference of the emitted light waves will occur due the various scattering centers (Figure 3.6b). Thus a non-isotropic angular dependency of the scattering light intensity is observed for these particles. The interference pattern of intraparticular scattered light is characteristic for the particle size and shape providing quantitative information of particles in very dilute solution by light scattering.

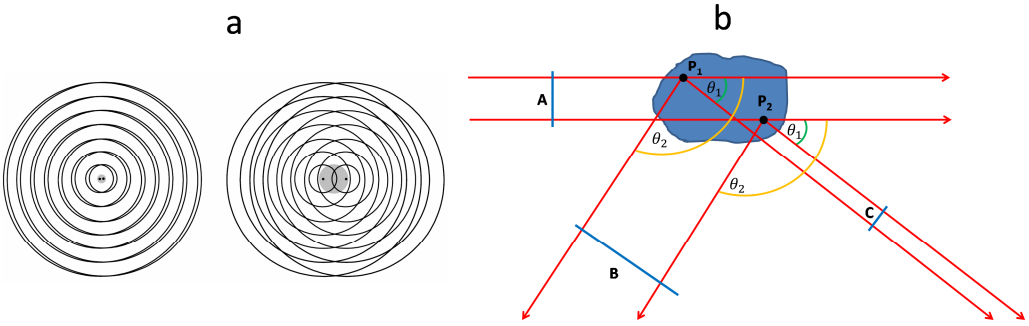

Figure 3.6. (**a**) the interference pattern of light scattered from small particles (left) and from larger particles (right). (**b**) light scattered from different regions of a scatterer with dimensions bigger than the wavelength of the scattered light. As an examples two scattering points, P_1 and P_2 are shown. At plane A all the incident light is in phase. Plane B and C is drawn perpendicular to the light which is scattered at angle θ_2 and θ_1 from the incident beam. The length difference AP_1C - AP_2C at small angle (θ_1) is shorter than AP_2B – AP_1B at larger

angles (θ_2). Therefore, larger the observation angle greater will be the phase differences in the light and the interference effect on the scattering intensity.

3.3.1. Static light scattering

According to aforementioned, scattered light is produced from an oscillating electric dipole due the interaction between electromagnetic waves and matter. To describe the nature of the intensity of the light detected in an experiment of light scattering some theoretical background considerations are needed. Firstly, we should start with the relation between the electric dipole moment and the electric field that is given by the equation 3.5. The electric dipole momentum $\vec{m}$ depends on electric field vector $\vec{E}$ of the incident radiation and polarizability α according:

$$\vec{m} = \alpha\vec{E} \qquad (3.5)$$

whereas, $\vec{E}$ is defined as:

$$\overrightarrow{|E|} = E_0 \exp(i(2\pi\nu t - kx)) \qquad (3.6)$$

where $\nu = \frac{c}{\lambda}$ is the frequency of light of wavelength λ, c is the speed of light in vacuum and $|\vec{k}| = k = 2\pi/\lambda$ the length of the wave vector. Assuming a vertically polarized incident light propagating into x-direction, the electrical field vector of the scattered light wave emitted by the oscillating dipole is described by:

$$E_s = \left(\frac{\partial^2 m}{\partial t^2}\right)\frac{1}{r_d c^2} = \frac{-4\pi^2\nu^2\alpha E_0}{r_d c^2}\exp\left(i\left(2\pi\nu t - \vec{k}r_D\right)\right) \qquad (3.7)$$

where, $\overrightarrow{r_D}$ is the distance vector from the scattering sample to the detector. Finally $|E_s|^2$ that is equal the scattering intensity (I_s) is detected.

For very dilute solutions of small particles (sizes smaller than λ/20), the scattering intensity is independent of the scattering angle and is only dependent on the scattering power of the dissolved particles b, their mass concentration c and the osmotic pressure π according to:

$$I \sim b^2 kT \frac{c}{\left(\frac{\partial\pi}{\partial c}\right)_{T,N}} \qquad (3.8)$$

The scattering power of b^2 depends on the difference in polarizability of solute and solvent that is related to the refractive index increment according to:

$$\left(\frac{dn}{dc}\right) \simeq \frac{n_D - n_{D,0}}{c} \qquad (3.9)$$

where n_D is the refractive index of the solute and $n_{D,0}$ the refractive index of the solvent. b^2 is also called contrast factor K and can be expressed as:

$$b^2 = \frac{4\pi^2 n_{D,0}^2 \left(\frac{dn}{dc}\right)^2}{\lambda_0^4 N_A} = K \text{ in cm}^2\text{g}^{-2}\text{Mol} \qquad (3.10)$$

where N_A is Avogadro number, π is the mathematical constant and λ_0 is the wavelength of the incident light. Since the scattering intensity in equation 3.7 depends on the experimental setup (eg. the sample-detector distance) the so-called Rayleigh ratio R_θ is used to normalize and eliminate any scattering dependence derived from these conditions such as scattering volume V or sample-detector distance r_D according to:

$$R_\theta = b^2 = \frac{4\pi^2 n_{D,0}^2 \left(\frac{dn}{dc}\right)^2}{\lambda_0^4 N_A} \frac{cM}{N_A} = (I_{solution} - I_{solvent}) \frac{r_D^2}{V} \qquad (3.11)$$

In the practice, R_θ is experimentally determined measuring the intensity of the scattered light by the solution ($I_{solution}$) and the pure solvent ($I_{solvent}$) at a specific angle θ in relation to the absolute scattering intensity of a standard solvent $I_{standard}$ (usually toluene) and renormalize this value by the Rayleigh scattering of the standard, $R_{standard}$:

$$R_\theta = \left(\frac{I_{solution} - I_{solvent}}{I_{standard}}\right) R_{standard} \qquad (3.12)$$

Equation 3.8 is derived from the fluctuation theory, $\left(\frac{d\mu}{dc}\right) = \frac{M_0}{\rho_0}\left(\frac{d\pi}{dc}\right)$, where μ is the chemical potential of the solvent in the solution, M_0 the molar mass of the solvent molecules and ρ_0 the solvent density. According to van't Hoff, for real solutions the molar mass (M_w) and the second virial coefficient (A_2) can be calculated using the following equation:

$$\frac{\partial \pi}{\partial c} = kT\left(\frac{1}{M_w} + 2A_2c + \cdots\right) \quad (3.13)$$

Therefore, rewriting the equation 3.11 for real solutions according to equation 3.13 gives the basic equation for static light scattering of small particles in solution:

$$\frac{Kc}{R_\theta} = \frac{1}{M_w} + 2A_2c + \ldots \quad (3.14)$$

However, for larger particles (sizes bigger than λ/20) the scattering intensity is no longer independent of the scattering angle (see figure 3.6b, in section 3.3). The angular dependence of the measured scattered intensity caused by the intraparticular interferences from the several scattering centers gives rise to the particle form factor $P(q)$:

$$P(q) = 1 - \left(\frac{qR_G}{3}\right)^2 \quad (3.15)$$

where R_G is the radius of gyration and q is the scattering vector defined by

$$q = \frac{4\pi n_0}{\lambda_0} sin\left(\frac{\theta}{2}\right) \quad (3.16)$$

n_0 is the refraction index of the solution where the particles are immersed and θ is the scattering angle. Inserting the $P(q)$ from equation 3.15 in equation 3.14 the very important Zimm equation is obtained:

$$\frac{Kc}{R_\theta} = \frac{1}{M_w}\left(1 + \frac{q^2R_G^2}{3}\right) + 2A_2c \quad (3.17)$$

The Zimm equation provides information about the sample molar mass (M_w), radius of gyration (R_G) and the second virial coefficient (A_2). A_2 provides important information related to the type of interactions between the solute and the solvent. When A_2 presents positive values the solute is immersed in a good solvent, otherwise, if A_2 assumes negative values the solute interaction is preferential and the solvent is considered to be a bad solvent. When no preferential interactions occur between solute and solvent the A_2 assumes values around zero.

3.3.2. Dynamic Light scattering

Particles in solution are constantly moving under the effect of the so-called Brownian motion caused by the thermal density fluctuation of the solvent. The scattering intensity resulted from the illumination of these moving particles fluctuates in function of time because of a change in the interference pattern with changing interparticle position (Fig. 3.7).

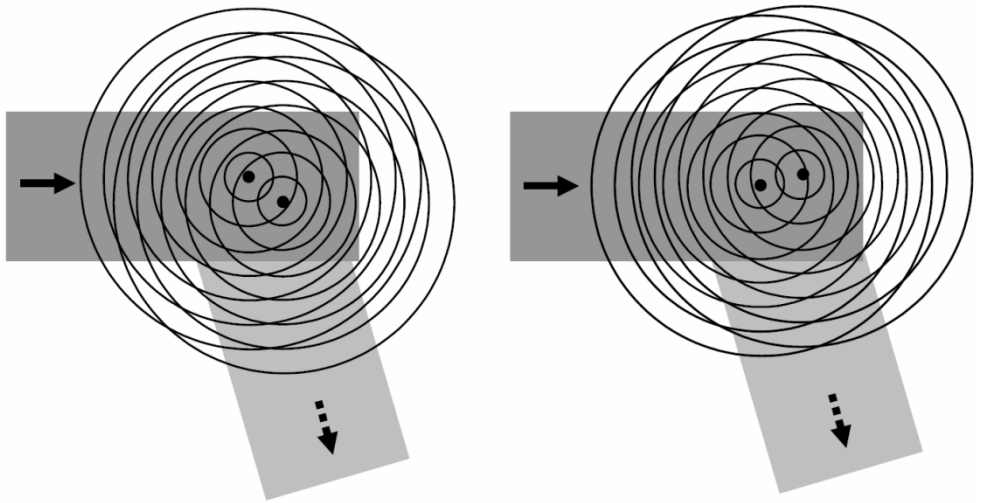

Figure 3.7. Representation of the change in the interference pattern of scattered intensity with time caused by Brownian motion of two scattering particles.[55]

Usually, to determine the particle mobility by light scattering the intensity fluctuation of the scattering light is expressed in terms of correlation functions. In the experimental setup the number of photons that reach the detector is recorded and analyzed by digital correlator and the signal is captured as time correlation function.

$$g_2(t) = \lim_{T\to\infty}\left[\frac{1}{T}\int_0^T I(t')I(t'+t)dt'\right] \qquad (3.18)$$

The subscript "2" in equation 3.18 indicates a correlation function of second order representing the scattering intensity proportional to the square of the electric field. The function g_2(t) can be related with the correlation function of the electric field through the Siegert[56] relation:

$$g_2(t) = 1 + \beta|g_1(t)|^2 \qquad (3.19)$$

where β is an instrumental parameter. The equation 3.19 is valid for ergodic system at finite concentration where the particles do not interact.

In several cases, g_1(t) is related to a simple exponential function:

$$g_1(t) = \exp(-\Gamma t) \quad (3.20)$$

where Γ is the decay rate related to relaxation time of the particle movement. However, scattering from real systems consisting of polydisperse objects fluctuates around an average value. One easy method for analyzing the polydipersity of such particle systems is the cumulant method represented by a polynomial:

$$g_1(t) = Aexp(-\bar{\Gamma}t)\left(1 + \frac{1}{2!}\mu_2 t^2 + \dots\right) \quad (3.21)$$

where A corresponds to the amplitude of the distribution, $\bar{\Gamma}$ is the average decay rate and μ_2 is the second cumulant that corresponds to width of the distribution. Through this method is possible to estimate the polydispersity index (PDI):

$$PDI = \frac{\mu_2}{\bar{\Gamma}^2} \approx \frac{M_w/M_n - 1}{4} \quad (3.22)$$

The method is valid for the systems where PDI<0.3 otherwise nonlinear methods of analysis must be employed and the correlation functions are treated using the mathematical operation inverse Laplace transformation according to equation 3.23:

$$g_2(t) - 1 = \beta[\int A(\tau)\exp(-t/\tau)d\tau\,]^2 \quad (3.23)$$

The inverse Laplace transformation is done by commercial software such as CONTIN[57] or REPES incorporated in the Gendist[58] program. The result of the transformation $A(\tau)$ is a distribution of relaxation times τ ($\Gamma = \tau^{-1}$) which can present one or several peaks representing one or more population of particles in the sample (Fig. 3.8).

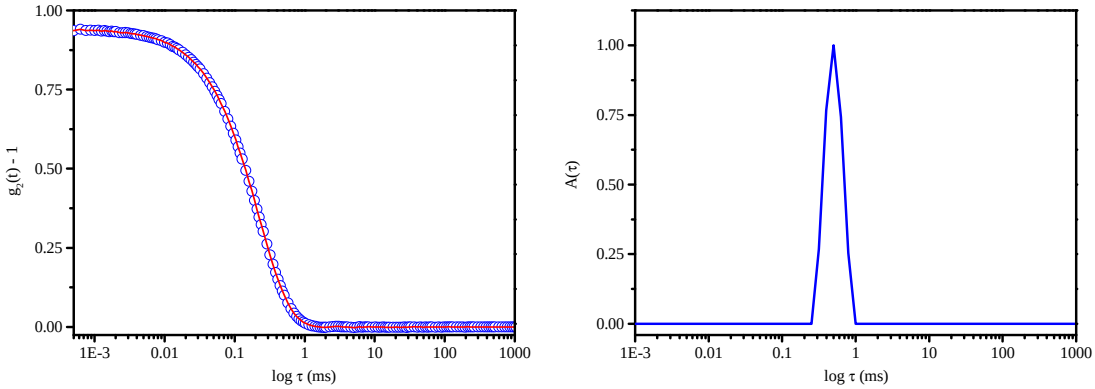

Figure 3.8. Time correlation function (left) and the distribution of relaxation times (right) obtained with REPES software. The red curve in the left picture corresponds to the fit of the correlation function using the method of cumulants.

From the Γ value the diffusion coefficient (D) of the particle can be determined using the relation with the scattering vector (q):

$$D = \frac{\Gamma}{q^2} \qquad (3.24)$$

Finally, from the diffusion coefficient value is possible to determine the hydrodynamic radius (R_H) of the particle, once the solvent viscosity (η) and the temperature (T) are known. In the equation 3.25, k_B is the Boltzmann constant (1.38×10^{-23} J K^{-1}).

$$R_H = \frac{k_B T}{6\pi\eta D} \qquad (3.25)$$

3.3.3 The ρ-ratio

The so-called ρ-ratio is an experimental quantity derived from combining the particles size characteristics determined from static and dynamic light scattering measurements. It provides indication of the scattering particle topology and is simply defined as:

$$\rho = \frac{R_G}{R_H} \qquad (3.26)$$

Table 3.1 shows the theoretical ρ values for the most important topologies.

Table 3.1. ρ-ratio for the most-typical particle morphologies

Topology	ρ-ratio
Homogeneous sphere	0.775
Hollow sphere	1
Ellipsoid	0.775 - 4
Random polymer coil	1.505
Cylinder of length l, diameter D	$\frac{1}{\sqrt{3}} \cdot \ln\left(\frac{l}{D} - 0.5\right)$

3.4 Electrophoretic light scattering (ELS)

The ELS measurements were employed in order to determine the average zeta potential (ζ) of the nanoparticles, which was done by using the Zetasizer Nano ZS instrument (Malvern Instruments, UK). The equipment measures the electrophoretic mobility (UE) and converts the value to ζ-potential (mV) through Henry's equation. Henry's function was calculated through the Smoluchowski approximation. The measurements were performed at 25 °C and the reported ζ-potential values are the average of 10 measurements.

The fixed aqueous layer thickness (FALT) was calculated according to the Guy-Chapman theory.[59] Zeta potentials were measured in various NaCl concentrations and plotted against *k*, with k^{-1} being the Debye-length, that is, $3.3\sqrt{c + 0.0053}$ (*c* is the concentration of NaCl). Therefore, by plotting ln ζ vs. *k*, the slope gives the thickness (*L*) of the adsorbed hydrophilic polymer layer.

3.5 Small angle X-ray scatteing (SAXS)

The SAXS technique is used to investigate structural details in the order of 0.5 to 100 nm. Compared with SLS, the SAXS technique presents three fundamental differences: they differ in the electromagnetic radiation wavelength (visible light present's wavelength between 380-700 nm whereas X-ray is between 0.01 to 0.2 nm); they differ in the scattering geometry (conventional SLS ranges from 20° to 150° whereas X-ray is from 0.5° to 4°); and in the origin of the nature of the scattering from the sample (once the light scattering in SLS is related to the differences in the refractive index between the solvent and the solute whereas

for X-ray the scattering intensity is related to the differences in the electron density in the sample system).

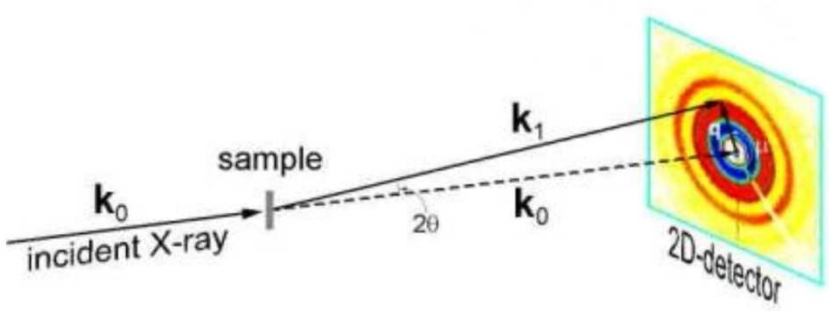

Fig. 3.9. Basic geometry of a SAXS experiment.

Figure 3.9 shows a classical geometry for a SAXS experiment. A collimated and monochromatic X-ray beam with variable wavelength focuses on the sample and the generated scattering is collected by a two-dimensional detector. During the experiment the number of photons in function of the scattering angle is measured. For the calculations of q in a SAXS experiment we use the aforementioned equation 3.16, using $n_0 = 1$.

The X-ray scattering intensity of a sample in function of q is given by[60]:

$$I_s(q) = \frac{N_s(q)}{t_s} = I_0(\lambda)\mathrm{A}\Delta\Omega\varepsilon T_s(\lambda)d_s\left(\frac{\partial\Sigma}{\partial\Omega}\right)(q) + BG \qquad (3.27)$$

where $I_s(q)$ is the quantity measured during an experiment and corresponds to the number of photons (N_s) of a given wavelength scattered through the angle (θ) that arrive on a small area of the detector per unit time (t_s). $I_0(\lambda)$ is the incident flux (in units of photons s^{-1} cm^{-2}), A is the area illuminated by the beam, $\Delta\Omega$ is the solid angle element defined by the size of a detector pixel, ε is the detector efficiency, $T_s(\lambda)$ is the transmission of the sample, d_s is the thickness of the sample, and BG is the scattering background. Finally, $(\partial\Sigma/\partial\Omega)$ is the differential scattering cross section (in units cm^{-1}); it is the quantity obtained from the absolute calibration of the measured intensity.

For a specific system the X-ray scattering intensity results from the multiplication of the form $P(q)$ and structure $S(q)$ factors according to the equation 3.28[61].

$$I(q) = NP(q)S(q) \qquad (3.28)$$

where N is the number of particles per unit volume. The form factor $P(q)$ is related to the scattering of a single isolated particle whereas the structure factor $S(q)$ is related to the scattering originating from the arrangement of the particles.

Generally, under the diluted regime the particles do not interact and the total scattering results from the sum of the scattering from the individual non-interacting particles. In this case significant information related to the particles shape and size can be extracted. On the other hand, when the system is composed of a large number of particles, the scattering intensity results from the contributions of $P(q)$ and $S(q)$. In this case, by applying mathematical treatment that include the theoretical profile of the contributions, $P(q)$ and $S(q)$ can be separated in the scattering spectra.

Taking into account that all the nanoparticles samples were measured under dilute regime, the structure factor $P(q)$ was modelled geometrically as homogenous spheres according to:

$$I(q) = V_p^2 \Delta\sigma^2 P(q,R)$$

$$= \left(\frac{4}{3}\pi R^3 \Delta\sigma\right)^2 \left(\frac{3[\sin(qR) - qR\cos(qR]}{(qR)^3}\right)^2 \qquad (3.29)$$

and the samples polydispersity was estimated using the log-normal distribution for which the probability density function is given by:

$$f(R,\mu,\delta) = \frac{1}{\sqrt{2\pi\delta R}} exp - \frac{\ln(R/\mu)^2}{2\delta^2} \qquad (3.30)$$

where R is the average radius, μ is the location parameter and δ^2 is the variance. The parameter δ is related to the standard deviation and gives the quantitative information about the width of the distribution.

3.6 Nanoparticles preparation

The details of the procedures for the preparation of each system are described in the appendices. One example is given for the preparation of the PBS/PBDL stealth nanoparticles

by nanoprecipitation (Chapter 6). The PBS/PBDL copolyester (5.0 mg.mL^{-1}) was firstly solubilized in acetone at 40 °C. Subsequently, the organic phase was drop-wise added (EW-74900-00, Cole-Parmer®) into a pre-heated (40 °C) 5% *v*/*v* ethanol/water mixture (20 mL) containing 0.00 mg.mL^{-1} (NP0), 0.25 mg.mL^{-1} (NP1:20 $w_{HPMA\text{-}chol}/w_{PBS/PBDL}$), 0.50 mg.mL^{-1} (NP1:10 $w_{HPMA\text{-}chol}/w_{PBS/PBDL}$), 0.75 mg.mL^{-1} (NP01:6.7 $w_{HPMA\text{-}chol}/w_{PBS/PBDL}$), 1.00 mg.mL^{-1} (NP1:5 $w_{HPMA\text{-}chol}/w_{PBS/PBDL}$) or 2.00 mg.mL^{-1} (NP1:2.5 $w_{HPMA\text{-}chol}/w_{PBS/PBDL}$) of dissolved ($R_H$ = 8.0 nm) PHPMA-chol free chains (Ultra-Turrax T25, IKA, Germany). The samples were left at room temperature for 2 h to achieve equilibrium structures and the organic solvent was further removed by evaporation under reduced pressure. The remaining free polymer chains were removed by washing the NPs solution several times using an Amicon Ultra-4 centrifugal filter with MWCO 30 kDa (Millipore, Czech Republic). The aqueous solutions were concentrated to the desired final concentrations and used immediately or stored at 4 °C. The DOX-loaded NPs were prepared by using essentially the same procedure except that in such a case 4.3 μmol of DOX.HCl and 12.9 μmol of triethylamine were dissolved in acetone along with the PBS/PBDL copolyester.

3.7 Paclitaxel (PTX) drug loading and loading efficiency

The total amount of the hydrophobic model drug paclitaxel (PTX) loaded into the NPs (total drug feeding subtracted from the free-drug amount collect after the ultrafiltration–centrifugation step described below) was measured by HPLC (Shimadzu, Japan) using a reverse-phase column Chromolith Performance RP-18e (100 × 4.6 mm, eluent water–acetonitrile with acetonitrile gradient 0–100 vol%, flow rate = 1.0 mL min^{-1}). To start, 100 μL of the drug-loaded NPs was collected from the bulk sample and diluted to 900 μL with acetonitrile. Afterwards, 20 μL of the final sample was injected through a sample loop. PTX was detected at 227 nm using ultraviolet (UV) detection. The retention time of PTX was 11.80 min in such experimental conditions. An analytical curve with linear response in the range (0.5–100 μg.mL^{-1}) was obtained and used to determined PTX contents. The free-drug was separated from the drug-loaded NPs by ultrafiltration–centrifugation (Ultrafree-MC 10 000 MW, Millipore) as detailed elsewhere.[62] The samples were centrifuged at 6000 rpm for 30 min. The amount of PTX in the nanoparticles was measured in the filtrate after the dissolution of NPs by using acetonitrile as described earlier. The drug-loading content (LC) and the drug-loading efficiency (LE) were calculated by using the following equations:

$$LC\ (\%) = \frac{drug\ amout\ in\ nanoparticles}{mass\ of\ nanoparticles} \times 100 \quad (3.31)$$

$$LE\ (\%) = \frac{drug\ amout\ in\ nanoparticles}{drug\ feeding} \times 100 \quad (3.32)$$

3.8 Determination of nanoparticles density

The average density of the nanoparticles (*d*) was estimated according to:

$$d = \frac{3M_{w(NP)}}{4\pi N_A (R_H)^3} \quad (3.33)$$

Where $M_{w(NP)}$ is the molecular weight of the nanoparticle calculated by equation 17, N_A is Avogadro's number and R_H is the nanoparticle hydrodynamic radius calculated according to the equation 25.

3.9 Cryo-Transmission Electron Microscopy (Cryo-TEM)

Cryo-TEM observations were performed to characterize the size and morphology of the polymeric nanoparticles. Thin liquid films of NP suspensions (0.5 wt% solid content) were prepared on NetMesh lacy carbon membranes (Pelco, U.S.A.) and quench-frozen in liquid ethane. Once mounted in a Gatan 626 cryo-holder cooled with liquid nitrogen, the samples were transferred to the microscope and observed at low temperature (-180 °C). The images were recorded on Kodak SO163 films using a CM200 Philips "Cryo" electron microscope operating at 80 kV. The negatives were digitized and the diameter of 650 particles was measured for each sample using the ImageJ software[63]. Number-, weight- and Z-average mean diameters ($\overline{D_N}$, $\overline{D_W}$ and $\overline{D_Z}$, respectively), as well as a polydispersity index P_{TEM}, were calculated as:

$$\overline{D_N} = \frac{\sum_i N_i D_i}{\sum_i N_i};\ \overline{D_W} = \frac{\sum_i N_i D_i^4}{\sum_i N_i D_i^3};\ \overline{D_Z} = \frac{\sum_i N_i D_i^6}{\sum_i N_i D_i^5} \quad (3.34)$$

$$P_{TEM} = \frac{\overline{D}_W}{\overline{D}_N} \quad (3.35)$$

3.10 References

[1] A.-C. Albertsson, I. K. Varma, *Adv. Polym. Sci.*, **2002**, *157*, 1.

[2] A.-C. Albertsson, I. K. Varma, *Biomacromolecules*, **2003**, *4*, 1466.

[3] R. Jain, N. H. Shah, A. W. Malick, C. T. Rhodes, *Drug Dev. Ind. Pharm.*, **1998**, 24, 703.

[4] T. K. Dash, V. B. Konkimalla, *J. Control. Release*, **2012**, 158, 15.

[5] M. A. Woodruff, D. W. Hutmacher, *Prog. Polym. Sci.*, **2010**, 35, 1217.

[6] D. Garlotta, *J. Polym. Environ.*, 2001, 9, 63.

[7] J.-M. Raquez, Y. Habibi, M. Murariu, P. Dubois, *Prog. Polym. Sci.*, **2013**, *38*, 1504.

[8] F. Danhier, E. Ansorena, J. M. Silva, R. Coco, A. L. Breton, V. Préat, *J. Control. Release*, **2012**, *161*, 505.

[9] S. B. Idris, S. Danmark, A. Finne-Wistrand, K. Arvidson, A. C. Albertsson, A. I. Bolstad, K. Mustafa, *J. Bioact. Compat. Pol.*, **2010**, *25*, 567.

[10] J. M. Anderson, M. S. Shive, *Adv. Drug Deliver. Rev.*, **2012**, *64*, 72.

[11] E. Pamula, P. Dobrzynski, B. Szot, M. Kretek, J. Krawciow, B. Plytycz, M. Chadzinska, *J. Biomed. Mater. Res. Part A*, **2008**, *87*, 524.

[12] P. T. Knight, J. T. Kirk, J. M. Anderson, P. T. Mather, *J. Biomed. Mater. Res. Part A*, 2010, 94A, 333.

[13] R. Chandra, R. Rustgi, *Prog. Polym. Sci.*, **1998**, *23*, 1273.

[14] L. S. Nair, C. T. Laurencin, Prog. Polym. Sci. **2007**, *32*, 762.

[15] M. Vert, S. M. Li, G. Spenlehauer, P. Guerin, *J. Mater. Sci: Mater. Medic.*, **1992**, *3*, 432.

[16] M. Sokolsky-Papkov, K. Agashi, A. Olaye, K. Shakesheff, A. J. Domb, *Adv. Drug Deliver. Rev.*, **2007**, *59*, 187.

[17] J. D. Kretlow, L. Klouda, A. G. Mikos, *Adv. Drug Deliver. Rev.*, **2007**, *59*, 263.

[18] Z. Pan, J. Ding, *Interface Focus*, **2012**, *2*, 366.

[19] C. Bartus, C. W. Hanke, E. Daro-Kaftan, *Dermatol. Surg.*, **2013**, *39*, 698.

[20] J. Panyam, V. Labhasetwar, *Adv. Drug Deliver. Rev.*, **2012**, *64*, 61.

[21] S. H. Bakhru, S. Furtado, A. P. Morello, E. Mathiowitz, *Adv. Drug Deliver. Rev.*, **2013**, *65*, 811.

[22] J. K. Vasir, V. Labhasetwar, *Adv. Drug Deliver. Rev.*, **2007**, *59*, 718.

[23] S. Acharya, S. K. Sahoo, *Adv. Drug Deliver. Rev.*, **2011**, *63*, 170.

[24] H. Li, J. Chang, A. Cao, J. Wang, *Macromol. Biosci.*, **2005**, *5*, 433.

[25] J. Yang, W. Tian, Q. Li, Y. Li, A. Cao, *Biomacromolecules*, **2004**, *5*, 2258.

[26] I. Bechthold, K. Bretz, S. Kabasci, R. Kopitzky, A. Springer, *Chem. Eng. Technol.*, **2008**, *31*, 647.

[27] J. Xu, B.-H. Guo, "Microbial Succinic Acid, Its Polymer Poly(butylene succinate), and Applications", in *Plastics from Bacteria: Natural Functions and Applications*, Springer-Verlag Berlin, Heidelberg, 2010, p. 347.

[28] R. van Dijkhuizen-Radersma, J. R. Roosma, P. Kaim, S. Metairie, F. L. A. M. A. Péters, J. de Wijn, P. G. Zijlstra, K. de Groot, J. M. Bezemer, *J. Biomed. Mater. Res.*, **2003**, *67A*, 1294.

[29] R. van Dijkhuizen-Radersma, J. R. Roosma, J. Sohier, F. L. A. M. A. Péters, M. van den Doel, C. A. van Blitterswijk, K. de Groot, J. M. Bezemer, *J. Biomed. Mater. Res.*, **2004**, *71A*, 118.

[30] L. Wang, J. Chen, H. Liu, Z. Chen, Y. Zhang, C. Wang, Z. Feng, *Polym. Int.*, **2004**, *53*, 2145.

[31] A. Lindström, A. C. Albertsson, M. Hakkarainen, *Polym. Degrad. Stab.*, **2004**, *83*, 487.

[32] J. Bremer, H. Osmandsen, "Fatty acid oxidation and its regulation" in *New Comprehensive Biochemistry: Fatty acid metabolism and its regulation*, Elsevier, Amsterdam, 1984, p. 113.

[33] A. J. Domb, M. Maniar, *J. Polym. Sci. Part A Polym. Chem*, **1993**, *31*, 1275-1285.

[34] J. P. Jain, M. Sokolsky, N. Kumar, A. J. Domb, *Polym. Rev.* **2008**, *48*, 156-191.

[35] A. Jäger, D. Gromadzki, E. Jäger, F. C. Giacomelli, A. Kozlowska, L. Kobera, J. Brus, B. Rihova, M. El Fray, K. Ulbrich, P. Štěpánek, *Soft Matter*, **2012**, *8*, 4343.

[36] E. Jäger, A. Jäger, T. Etrych, F. C. Giacomelli, P. Chytil, A. Jigounov, J.-L. Putaux, B. Říhová, K. Ulbrich, P. Štěpánek, *Soft Matter*, **2012**, *8*, 9563.

[37] E. Jäger, A. Jäger, P. Chytil, T. Etrych, B. Říhova, F. C. Giacomelli, P. Štěpáanek and K. Ulbrich, *J. Control. Release*, **2013**, *165*, 153.

[38] A. C. Albertsson, I. K. Varma, Aliphatic polyesters, *Biopolymers Online*, **2005**, Part 4. Polyesters.

[39] U. Edlund, A.-C. Albertsson, *Adv. Drug Deliver. Rev.*, **2003**, 55, 585.

[40] A. Duda, S. Penczek, Mechanisms of aliphatic polyester Formation, *Biopolymers Online*, **2005**, Part 4. Polyesters.

[41] A.-C. Albertsson, I. K. Varma, "Aliphatic Polyesters: Synthesis, Properties and Applications" in *Advances in Polymer Science 157: Degradable Aliphatic Polyesters*, Springer-Verlag Berlin, Heidelberg, 2002, p. 4.

[42] W. H. Carothers, *Trans. Faraday Soc.*, **1936**, *32*, 39.

[43] W. H. Carothers, *J. Am. Chem. Soc.*, **1929**, *51*, 2548.

[44] N. Bikiaris, D.S. Achilias, *Polymer*, **2006**, *47*, 4851.

[45] N. Bikiaris, D.S. Achilias, *Polymer*, **2008**, *49*, 3677.

[46] J. Yang, S. Zhang, X. Liu, A. Cao, *Polym. Degrad. Stabil.*, **2003**, *81*, 1.

[47] S. Luo, F. Li, J. Yu, A. Cao, *J. Appl. Polym. Sci.*, **2010**, *115*, 2203.

[48] N. Jacquel, F. Freyermouth, F. Fenouillot, A. Rousseau, J. P. Pascault, P. Fuertes, R. Saint-Loup, *J. Polym. Sci. Pol. Chem.*, **2011**, *49*, 5301.

[49] A. Gallardo, J. S. Roman, P. J. Dijkstra, J. Feijen, *Macromolecules*, **1998**, *31*, 7187.

[50] C. Jérôme, P. Lecomte, *Adv. Drug Deliver. Rev*, **2008**, *60*, 1056.

[51] P. Lecomte, R. Jérôme, "New developments in the synthesis of aliphatic polyesters by ring-opening polymerization" in *Biodegradable Polymers for Polymer Industrial Applications*, Woodhead Publishing Ltd, Cambridge, 2005, pp. 77.

[52] P. Lecomte, R. Jérôme, *Adv. Polym. Sci.*, **2012**, *245*, 173.

[53] S. Penczek, M. Cypryk, A. Duda, P. Kubisa, S. Slomkowski, *Prog. Polym. Sci.*, **2007**, *32*, 247–282.

[59] J. Weiner, P.-T Ho, " Light-Matter interaction", John Wiley & Sons, Hoboken, New Jersey, 2003.

[60] W. Schärtl, "Light Scattering from Polymer Solutions and Nanoparticle Dispersions", Srpinger-Verlang, Berlin, 2007.

[61] P. Štěpánek, In *Dynamic light scattering: The Method and Some Applications;* Brown, W., Ed.; Oxford Science Publications: Oxford, 1993.

[62] S. W. Provencher, *Comp. Phys. Commun*. **1982**, *27*, 229.

[63] J. Jakes, *Collect. Czech Chem. Commun.* **1995**, *60*, 1781.

[59] J. N. Israelachivili, in *Inntermolecular and Surface Force*, Academic Press, London, 1985.

[64] C. A. Dreiss, K. S. Jack, A. P. Parker, *J. Appl. Cryst.*, **2006**, *39*, 32.

[65] A. F. Craievich, *Mater. Res.* **2002**, *5*,1.

[62] E. Penott-Chang, A. Walther, P. Millard, A. Jäger, E. Jäger, A. H. E. Müller, S. S. Guterres and A. R. Pohlmann, *J. Biomed. Nanotech.*, **2012**, *8*, 272-279.

[63]http://rsbweb.nih.gov/ij/

4. Physicochemical aspects behind the size distribution of biodegradable polymer nanoparticles

4.1 Introduction

According to aforementioned, polymer nanoparticles (NP) can provide a crucial advantage to various drugs and therapeutic biological molecules by improving their efficacy and reducing potential toxic and side effects, by protecting the therapeutic agents against degradation and by controlling their release. Among the particles physicochemical properties such as composition, morphology and surface properties, the size of the nanoparticle is a crucial parameter in systems designed for drug release applications. In intravenous administration the nanoparticle size strongly influences the biodistribution and pharmacokinetics of the drugs.[1,2,3,4,5,6,7] It has been shown that the clearance of the smaller particles (~80 nm) from the bloodstream was slower than that of bigger particles (~200 nm). Moreover, filtration of nanoparticles by the spleen and trapping in the hepatic parenchyma also depended on size.[5] Therefore, the size and the size distribution of nanoparticles need to be accurately controlled for efficient and safe drug delivery.

There are several methodologies employed in the preparation of polymer nanoparticles intended to biomedical applications.[8,9,10,11,12,13,14,15] Conventionally, they are divided in two general methods: (1) the polymerization and polycondensation of monomers, and (2) the dispersion of preformed polymers. In the dispersion of preformed polymers, the choice of the preparation method for nanocarriers mainly depends on the employed polymeric materials. For the self-assembly of polymers or copolymers in aqueous solution, the emulsion-solvent evaporation process and the nanoprecipitation technique (solvent shifting) are the more often described.[16,17,18] They are characterized by procedural simplicity, high encapsulation efficiency, high reproducibility, low possible contaminant content, low cost and easy up-scaling.[19,20,21,22,23,24,25] As mentioned in the introduction, nanoprecipitation was the technique of choice to produce the nanocarriers described in this thesis. The purpose of this approach, e.g. easy tuning of particles size, and some physico-chemical findings are described and discussed throughout this chapter.

4.2 The parameters involved in the nanoprecipitation of polymers

There are several physicochemical parameters involved in the nanoprecipitation of polymers that influence the final particles size and size-distribution.[18,26,27] Some of the most relevant physicochemical parameters of nanoprecipitation were evaluated in detail using as a model the well-known biocompatible and biodegradable poly(lactic-co-glycolic acid) PLGA copolymer.[28] The influence of the physicochemical properties of the aqueous and organic

phase during the preparation of biodegradable NPs as well as physicochemical aspects behind the size and size-distribution of NPs have been investigated and the results are summarized below.

4.2.1 The influence of the polymer concentration

The polymer concentration was tested from 1.4 to 15 mg.mL^{-1} and their influence in the size, size-distribution and ζ-potential of the prepared NPs at preset acetone/water ratio (0.4) is portrayed in Fig. 4.1. As previously observed,[29,30,31,32] the increase in polymer concentration resulted in increase in the mean particle size. The more widespread explanation to the particles growth are related to the classical nucleation and growth mechanism applied to low molecular weight compounds.[33,34,35] In this mechanism, a few critical nuclei of pure solute are formed when the anti-solvent is added to the solvent solution causing solute super saturation due to the fluctuations in the solvent concentration. These critical nuclei grow by capturing solute molecules from the surrounding solution. The signature of the nucleation and growth mechanism is that the number of particles remains equal to the number of nuclei (Fig. 4.2,).[33] At the end of growth, the mass per particle equals the solute mass concentration divided by the number concentration of particles. Since the number of nuclei varies exponentially with the supersaturation, one should expect higher solute concentrations to yield a much higher number of nuclei and therefore smaller particles.

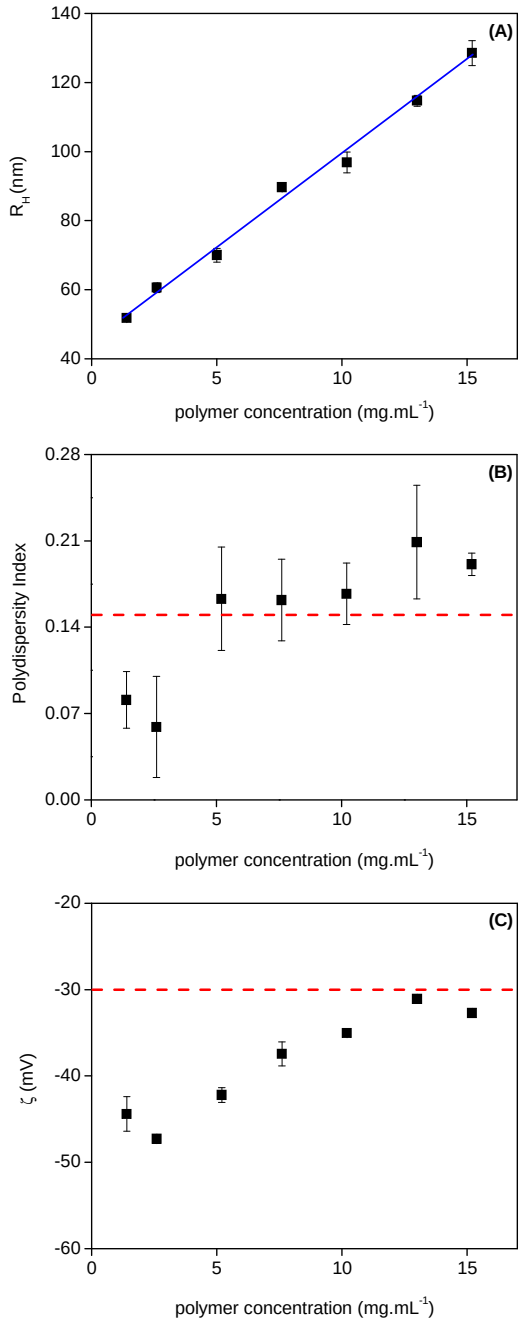

Figure 4.1. Influence of the polymer concentration on the structural features of PLGA nanoparticles prepared by nanoprecipitation: mean nanoparticle size (A), polydispersity index (B) and ζ-potential (C). The acetone:water ratio was preset to 0.4. (the read dashes expressed the acceptable limits for drug release systems)

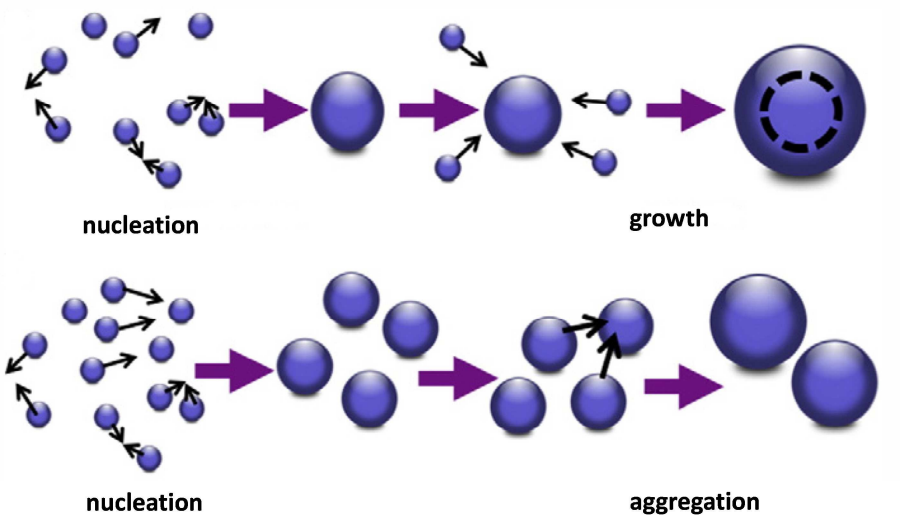

Figure 4.2. Schematic description of nucleation and growth mechanism (above), and nucleation and aggregation mechanism (below).[18]

In order to drive the nanoprecipitation process through the nucleation and growth mechanism homogenous supersaturation of the polymer solution must be achieved.[18] To obtain a homogenous supersaturation the mixing process between the aqueous and organic phases, and the associated molecular diffusion of components, must be much faster than the rate of nanoparticle nucleation.[36] This can be achieved just by using special devices that provide fast mixing conditions at very low polymer concentrations and solvent to non-solvent ratios.[37] However, the very low volumes of NPs produced by using such devices hinders the scale-up from laboratory to industrial application.

Under average conditions the nanoprecipitation process using pre-formed polymers produce NPs in which the size grows linearly with the polymer concentration (Fig. 4.1a).[29-32] In these cases NPs grow manly through nucleation and aggregation mechanism.[30] In addition to the nuclei growth under supersaturation, unavoidable nuclei aggregation due to the random encounters between the growing nuclei is also expected to occur (Fig. 4.2). Therefore, the increase in the number of available copolymer chains (higher concentration) leads to an increase in the number of nuclei and consequently in the probability of nuclei encounters.[30] Each encounter causes aggregation of nuclei thereby increasing the nanoparticle size. The NPs grow until the electrostatic repulsions stabilization quenches the aggregation process.[38,39,40] Moreover, the increase in the organic solution viscosity by the increase of the polymer concentration results in an increase in the mass transfer resistance. This causes a

reduction of the polymer-solvent diffusion into the external aqueous phase, larger nuclei are formed and consequently larger NPs.

The NPs size-distribution was also influenced by the polymer concentration (Fig. 4.1b) as observed previously.[31] The size-distribution became broad when bigger particles were obtained and it can be understood by considering the process of aggregation. At low polymer concentration the viscosity of the organic solution does not influence the mixing process and the nuclei formed during supersaturation are small and homogenous to some extent. When polymer concentration increases the viscosity starts to interfere in the mixing process increasing the nuclei size and inhomogeneity. The random aggregation of the heterogeneous nuclei generates a polydisperse distribution of NP sizes. Therefore, increase in polymer concentration increases the heterogeneity between the nuclei and the number of random aggregation steps resulting in bigger and more polydisperse NPs.[38,39] Furthermore, the Oswald ripening[41] cannot be ruled out in polydisperse systems since the increase in the polymer concentration enhances the difference between the growing nuclei.

Taking into account that the end-groups of the PLGA copolyester used in the production of the NPs is carboxylic acid terminated, the nature of the charge on the particles surface is related to the presence of these deprotonated ionic end-groups at the polymer/water interfaces.[40] Therefore, it is expected a negative zeta potential values of NPs prepared by polymers containing such end-groups.[16,18,40] The values of zeta potential in function of polymer concentration are shown in Fig. 4.2a. It is noted that with the increase in the polymer concentration the zeta potential is slightly displaced towards smaller absolute values. We speculate that this behavior might be related to the mixing process, once opposite trend for the zeta potential were observed when high speed mixer (Ultraturrax® T25 basic, IKA, Germany) was used at same conditions (Fig. 4.3) or when a Robot micropipeting system for low volumes was applied in the preparation of NPs.[31] Nevertheless, even for the highest concentration, the zeta potential is still more negative than –30 mV which is used as the limit for nanoparticle stability.[39,40]

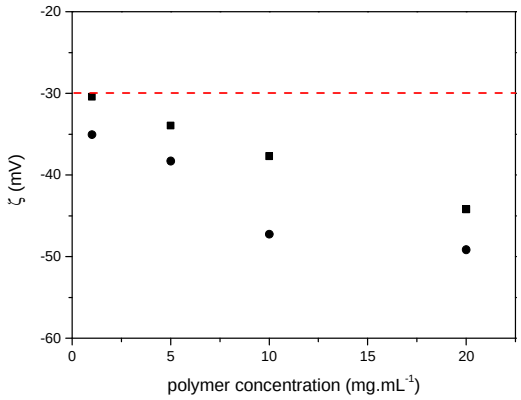

Figure 4.3. Influence of polymer concentration in the zeta potential under high speed stirring conditions; 3500 rpm (■) and 12 000 rpm (●).

4.2.2 The influence of the solvent/water ratio

The solvent/water ratio was varied from 0.2 to 1.0 at preset final polymer concentration of 1.4 mg.mL^{-1} (Fig. 4.4A). A small effect of the solvent/water ratio was observed on the size of the produced particles in the range from 0.4 to 1.0, although for 0.2 the manufactured NPs are substantially bigger. From the low solvent/water ratio region (0.2 to 0.8), the mean particle size decreases as the solvent/water ratio increases. The mean particle size was reduced from 67.8 nm to 44.0 nm as the solvent/water ratio increased from 0.2 to 0.8. Perevyazko et al.[31] investigated the influence of the organic fraction in the NPs size under several conditions: at constant initial concentration (1), at constant final polymer concentration (2), and at constant amount of the polymer in the final mixture (3). The results (Fig. 4.5) show that the points are similar to the parabolic shape of the curve found in our experiments (Fig. 4.4a).

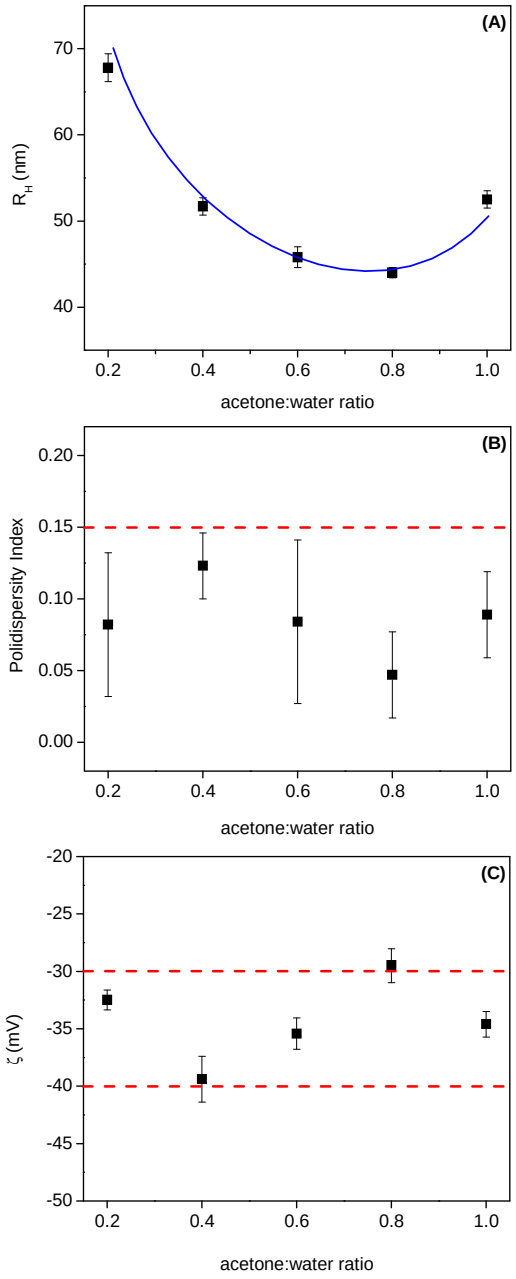

Figure 4.4. Influence of acetone/water ratio on the structural features of PLGA nanoparticles prepared by nanoprecipitation: mean nanoparticle size (A), polydispersity index (B) and ζ-potential (C). The polymer concentration was preset to 1.4 mg.mL^{-1}.

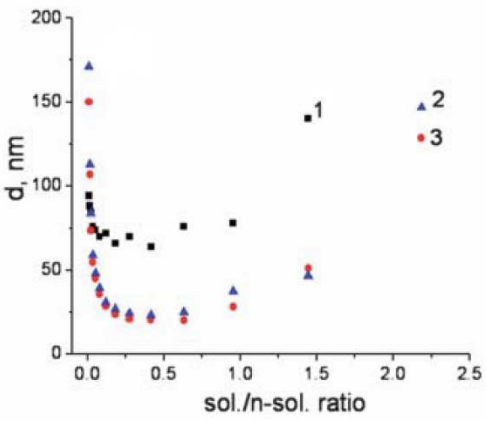

Figure 4.5. Dependence of the mean sizes of the formed particles on the solvent/non-solvent ratio where (1) the initial polymer concentration was kept constant at 3.57 mg.mL^{-1}, (2) polymer concentration in the final mixture was kept constant at 0.1 mg.mL^{-1}, and (3) amount of the polymer in the final mixture was kept constant at 0.1 mg (reproduced from reference 31).

The interpretations of the results were based on nucleation and aggregation and nucleation and growth mechanism. At low solvent/water ratios (< 0.2) the low amount of organic solvent hampers the formation of nucleation sites, thus the number of nuclei formed is small and the particle size is bigger. The increase in the volume fraction of the organic phase increases the number of nucleation sites, which leads to the formation of smaller particles. For our experimental setup the maximum number of nucleation sites appears close to the solvent/water ratio ~0.6–0.8. Beyond this ratio the NPs growth is no longer governed by nucleation and aggregation, since the superstation is very low and the nucleation events are rare. These nuclei are far apart from each other and their encounters are rare, therefore the few nuclei grow by collecting the remaining polymer chains by the nucleation and growth mechanism.[30]

In our case the polydispersity seems not to be affected by the solvent/water ratio since the produced PNPs are narrowly distributed in size as judged by the polydispersity index values always below 0.15 (Fig. 4B). In a similar way, no significant changes were observed in the zeta potential of the prepared PLGA NPs within the solvent/water ratio range studied (Fig. 4.4c). The determined values ranged randomly in a narrow window from −30.0 mV to−40.0 mV. The high surface charge of the NPs ($\zeta < -30.0$ mV) suggests good dispersion stability of the produced NPs and prevents their aggregation due to the existence of electric repulsion

forces. Consequently, the NPs prepared under these conditions showed good stability for months when stored at 4◦C.

4.2.3 The influence of the organic solvent

Many authors investigated the influence of the organic solvent on particle size.[42,43,44,45,46] They studied the influence of the physicochemical parameters such as the organic solvent dielectric constant,[42] solvent/water interactions,[43] solvent/water solubility parameter difference[44] and polymer–solvent interactions.[45,46]

In order to investigate the influence of the organic solvent the nanoprecipitation procedures were performed by using the following water miscible solvents: DMSO, DMF, acetone, acetonitrile and THF. The most relevant physicochemical parameters of these solvents are listed in Table 4.1. Fig. 4.6c depicts an example of the visual appearance of the suspensions for several solvents. The suspensions are fully transparent for DMF, weakly opalescent for acetone and completely opalescent for THF. As expected, the increase in suspension opalescence correlates well with the increase in the NPs size in function of the solvent type (Fig. 4.6b). Furthermore, the cumulant expansion fitted the curves reasonably well suggesting a monomodal distribution of nanoparticles ($\mu_2 / \Gamma^2 < 0.15$, Fig. 4.6a). The values of NPs sizes, polydispersity index and zeta potential are shown in Fig. 4.7.

Table 4.1. Physicochemical properties of solvents (at 25 ^{o}C) and polymers employed in the nanoprecipitation protocols: η (viscosity), ε (dielectric constant), δ (solubility parameter) and γ (surface tension).

Entry	η (mPa.s)	ε	γ (mN.m^{-1})	δ (Mpa$^{1/2}$)
Water	0.891	80.20	72.0	47.9
DMSO	1.987	47.24	42.9	26.4
DMF	0.794	38.25	36.4	24.7
Acetonitrile	0.369	36.64	28.7	24.3
Acetone	0.306	21.01	23.5	19.7
THF	0.456	7.52	27.1	18.5
PCL	-	-		20.4
PLGA	-	-		19.9

The comparison between the experimental data and the solvent physicochemical parameters (table 4.1) reveals that there is no correlation between the viscosity of the solvent and the final dimension of the NPs since by employing the solvent of highest viscosity (DMSO and DMF) the smallest NPs were produced (Fig. 4.8). Likewise, we could not find proper correlation between particle size and water-solvent interfacial tension (Fig. 4.9). Similar conclusions were described in a review by Mora-Huertas et al.[16] where several experimental data from the literature related to solvent properties such as density, viscosity and surface tension were compared with the particle size. On the other hand, for the thermodynamic solvent-water interaction parameter ($\chi_{\text{solvent-water}}$) the authors, in some cases, could found correlation with the particle size.[47,48] Some explanation was given in terms of total solvent-water miscibility which guarantees fast phase mixing making the impact of solvent diffusion irrelevant. Therefore, we evaluated the solvent-water compatibility through the $\chi_{\text{solvent-water}}$ parameter based on the Hildebrand solubility parameter (δ) (Table 4.1)

$$\chi_{\text{solvent-water}} = \frac{V_{\text{water}}}{RT}(\delta_{\text{solvent}} - \delta_{\text{water}})^2 \qquad (4.1)$$

The parameter $\chi_{\text{solvent-water}}$ describes the interaction between the molecules of water and the molecules of the organic solvent and V_{water} stands for the molar volume of water (calculated based on its molar mass and density), R being the gas constant, T the absolute temperature and δ_{water} and δ_{solvent} the solubility parameters of the water and organic solvent respectively. Fig. 4.7A shows the plot of mean particle size as a function of the interaction parameter. A consistent tendency was observed of size increase as a function of $\chi_{\text{solvent-water}}$, where the lower the $\chi_{\text{solvent-water}}$ the smaller the NPs. The mean particle size increases in the order: DMSO < DMF < acetonitrile < acetone < THF, from the smallest towards the highest $\chi_{\text{solvent-water}}$. The high water-solvent affinity allows higher water-solvent mixing rate leading to formation of smaller NPs. Since the diffusion-stranding phenomena between water-solvent mixture is a key parameter in the nucleation process, the water-solvent miscibility expressed by the $\chi_{\text{solvent-water}}$ is a direct indication of the quality of the solvent mixing involved in the process. It seems that lower the $\chi_{\text{solvent-water}}$ the smaller and faster are the formed nuclei during the nanoprecipitation. This confirms that water-solvent miscibility is of chief importance in the diffusion-stranding phenomenon and thus in the formation of NPs by nanoprecipitation.

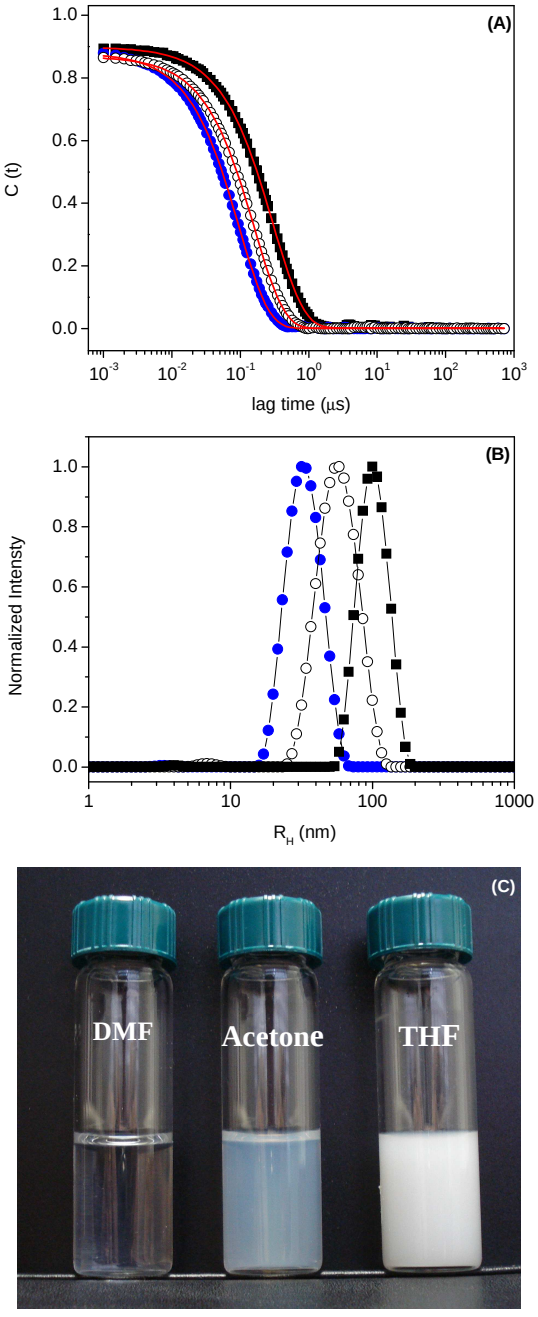

Figure 4.6. Autocorrelation functions measured at 173° and 25.0 °C (A), respective distributions of R_H revealed by the REPES algorithm (B) and the visual appearance of PLGA NPs produced from different organic solvents (C): DMF (●), acetone (○) and THF (■). The polymer concentration and the solvent/water ratio were preset to 1.4 mg mL^{-1} and 0.4. The solid lines in (A) correspond to the cumulant fittings.

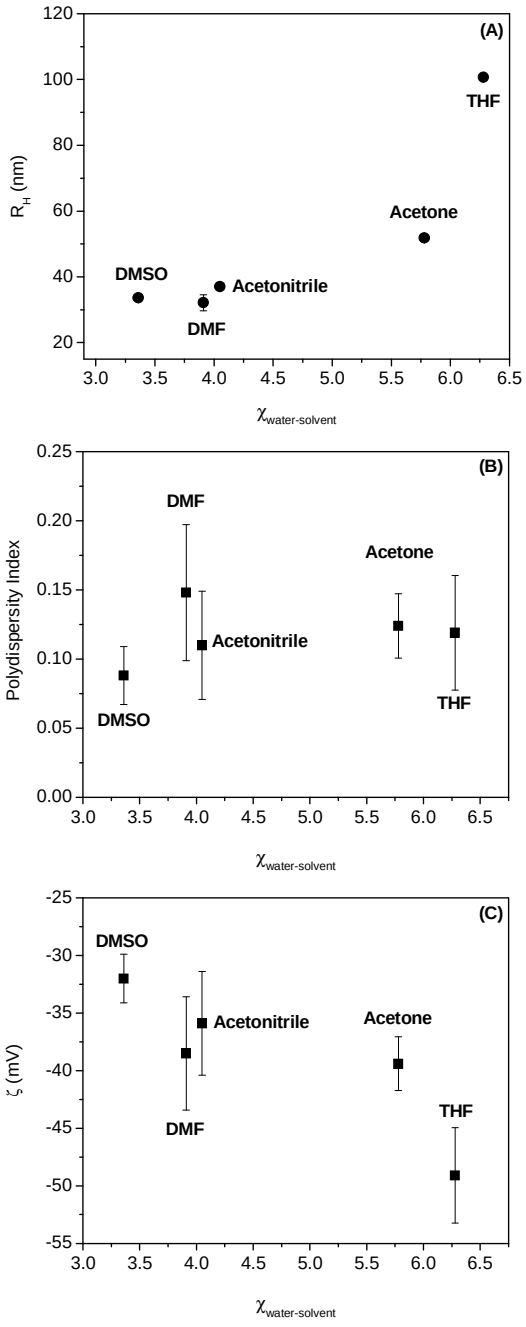

Figure 4.7. Influence of the water-organic solvent interaction parameter ($\chi_{water-solvent}$) on the mean nanoparticle size (A), polydispersity index (B) and ζ-potential (C) of PLGA nanoparticles prepared by nanoprecipitation. The polymer concentration and the solvent/water ratio were preset to 1.4 mg.mL^{-1} and 0.4, respectively.

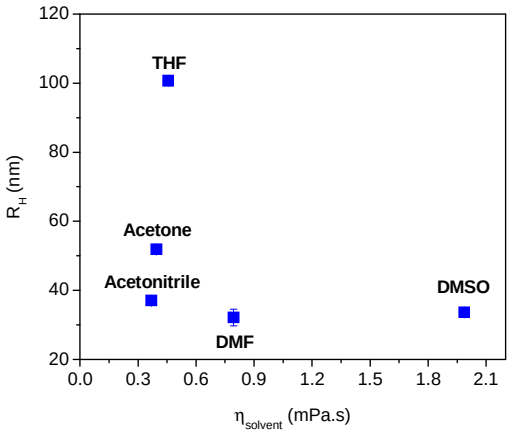

Figure 4.8. Influence of the solvent viscosity on the size of PLGA nanoparticles prepared by nanoprecipitation.

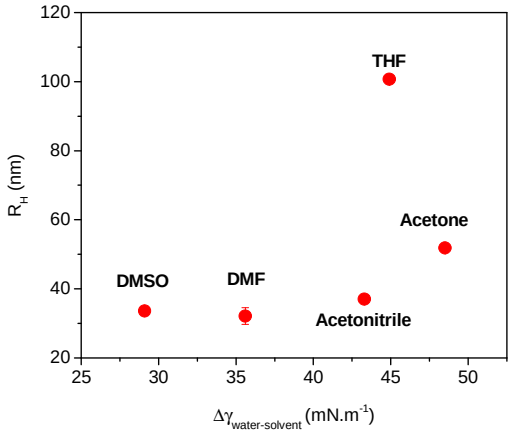

Figure 4.9. Influence of $\Delta\gamma_{water\text{-}solvent}$ on the size of PLGA nanoparticles prepared by nanoprecipitation.

When the polymeric NPs were manufactured using PCL and PBS/PBDL polymers (Fig. 4.10) at the same conditions using DMF, acetone and THF the particles size increases in the same order (DMF < acetone < THF, Table 4.2). We consider these results of fundamental importance because they clearly confirm that solvent–water interaction is one of the main factors affecting the mean NPs size independently of the nature of the biodegradable polymer.

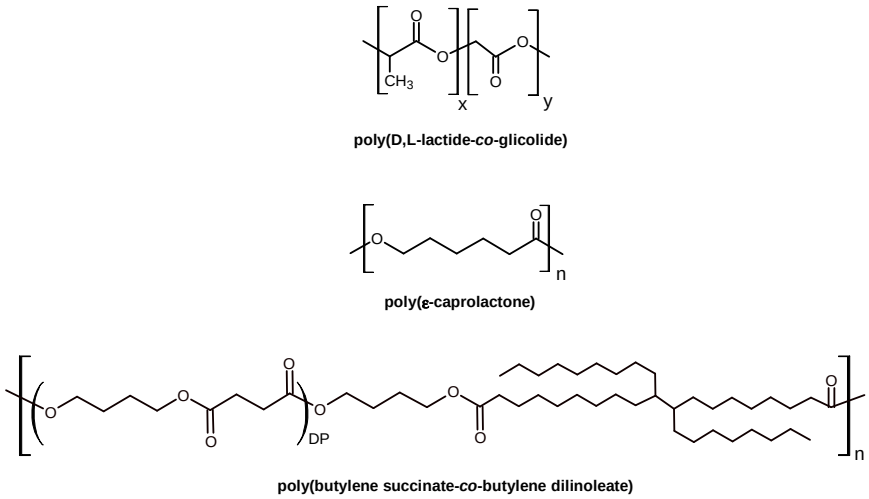

Figure 4.10. Polymer strucuture of PLGA, PCL and PBS/PBDL.

Regarding the polydispersity (Fig. 4.7B) and the ζ-potential (Fig. 4.7C) of the produced NPs no significative changes were observed as function of the nature of the organic solvent. The average values were always below 0.15 and -30 mV, respectively.

Although the correlation between intercation parameter (χ) and mean particle size not linear, we have found that the size of the NPs can be easily and precisely tuned in a linear way by using mixtures of solvent. For example, by mixing DMF and THF we were able to linearly tune the size of PLGA NPs from ~ 30 nm to ~100 nm keeping constant the polymer concentration. The same profile has been observed in mixtures of acetone and THF and the results are given in Fig 4.11. The same behavior was also evidenced in the manufacturing of NPs starting from different biodegradable polymers. The representative example for PBS/PBDL NPs is given in Figure 4.11c. These experimental evidences strongly suggest that the mean particle size depends chiefly on solvent/antisolvent interactions rather than on the other parameters, eg. solvent-polymer interactions.

Table 4.2. Mean particle size (R_H), polydispersity index and ζ-potential of a variety of polymeric nanoparticles prepared by nanoprecipitation from different starting organic solvents (polymer concentration 1.4 mg.mL^{-1}; solvent/water 0.4).

Polymer	Solvent	R_H (nm)	Polydispersity	ζ (mV)
PBS/PBDL	DMF	25.1	0.23	-36.8
	Acetone	49.1	0.03	-33.9
	THF	103.8	0.13	-37.4
PLGA	DMF	29.9	0.27	-38.5
	Acetone	52.1	0.12	-39.4
	THF	109.7	0.05	-49.1
PCL	DMF	63.9	0.24	-28.7
	Acetone	88.6	0.10	-23.0
	THF	212.1	0.28	-52.5

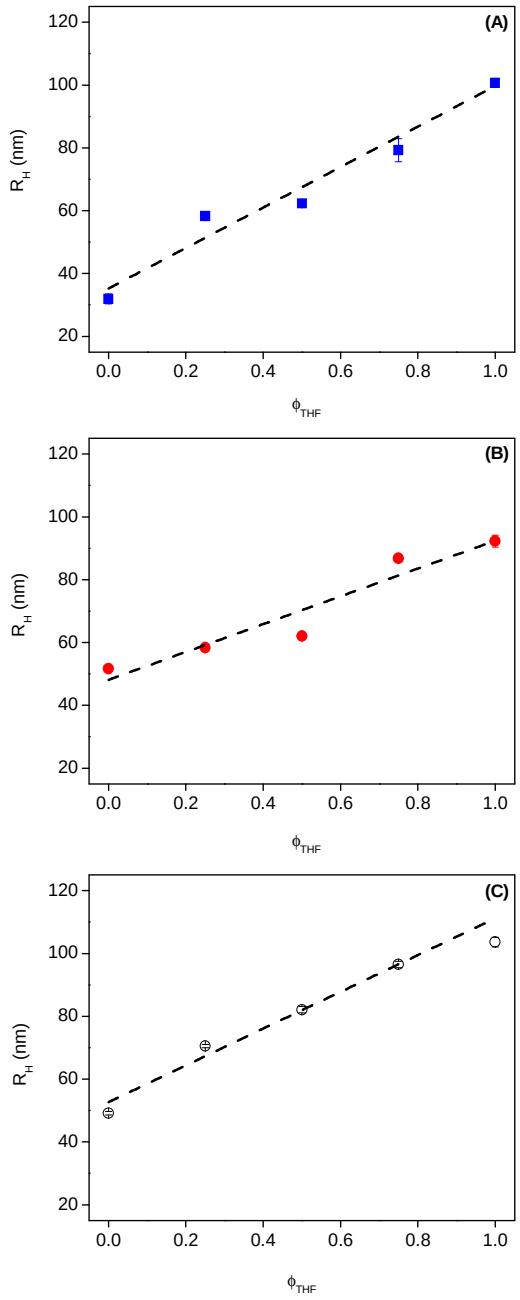

Figure 4.11. R_H of PLGA polymeric NPs prepared by nanoprecipitation as a function of the ϕ_{THF} in DMF/THF (A) and acetone/THF mixtures (B). R_H of PBS/PBDL polymeric nanoparticles prepared by nanoprecipitation as a function of the ϕ_{THF} in acetone/THF mixtures (C).

4.3. Conclusion

Some of the most relevant physicochemical parameters related to NPs size produced by nanoprecipitation process such as polymer concentration, solvent/anti-solvent ratio and the nature of the organic solvent were investigated in detail. NPs with hydrodynamic radius ranging from 28 to 128 nm were successfully produced through nanoprecipitation by manipulation of these parameters. Besides polymer concentration and solvent/anti-solvent ratio, the nature of the organic solvent seems to be the most relevant physicochemical parameter, because the size of the NPs can be precisely and linearly tuned in a wide size range by using solvent mixtures as organic phase without affecting the polydispersity and the ζ-potential.

4.4 References

[1] M. A. Dobrovolskaia, P. Aggarwal, J. B. Hall, S. E. McNeil, *Mol. Pharm.*, **2008**, *5*, 487.

[2] F. Lu, S. H. Wu, Y. Hung, C. Y. Mou, *Small*, **2009**, *5*, 1408.

[3] H. Lee, H. Fonge, B. Hoang, R.M. Reilly, C. Allen, *Mol. Pharm.* **2010**, *7*, 1195.

[4] S. Tender, D. Docter, S. Rosfa, A. Wlodarski, J. Kuharev, A. Rekik, S. K. Knauer, C. Bantz, T. Nawroth, C. Bier, J. Sirirattanapan , W. Mann , L. Treuel , R. Zellner , M. Maskos, H. Schild, R. H. Stauber, *ACS Nano*, **2011**, *5*, 7155.

[5] T. Maldiney, C. Richard, J. Seguin , N. Wattier , M. Bessodes, D. Scherman, *ACS Nano*, **2011**, *5*, 854.

[6] E. Vlashi, L. E. Kelderhouse, J. E. Sturgis, P. S. Low, *ACS Nano*, **2013**, 7, 8573.

[7] L. Shang, K. Nienhaus, G. U. Nienhaus, *Journal of Nanobiotechnology*, **2014**, *12*, 5.

[8] C. Allen, D. Maysinger, A. Eisenberg, *Colloid Surface B*, **1999**, *16*, 3.

[9] C. P. Reis, R. J. Neufeld, A. J. Ribeiro, F. Veiga, *Nanomedicine*, **2006**, *2*, 8.

[10] T. Akagi, M. Baba, M. Akashi, *Polymer*, **2007**, *48*, 6729.

[11] V. Lassalle, M. L. Ferreira, *Macromol. Biosci*. **2007**, *7*, 767.

[12] C. Vauthier, K. Bouchemal, *Pharm. Res.*, **2009**, *26*, 1025.

[13] A. Kumari, S. K. Yadav, S. C. Yadav, *Colloid Surface B*, **2010**,*75*, 1.

[14] J. P. Rao, K. E. Geckeler, *Prog. Polym. Sci.*, **2011**, *36*, 887.

[15] J. Nicolas, S. Mura, D. Brambilla, N. Mackiewicz, P. Couvreur, *Chem. Soc. Rev.*, **2012**, *42*, 1147.

[16] C. E. Mora-Huertas, H. Fessi, A. Elaissari, *Adv. Colloid Interfac. Sci.*, **2011**, *163*, 90.

[17] S. Schubert, J. T. Delaney Jr, U. S. Schubert, *Soft Matter*, **2011**, *7*, 1581.

[18] E. Lepeltier, C. Bourgaux, P. Couvreur, *Adv. Drug Deliver. Rev.*, **2014**, *71*, 86.

[19] D. Moinard, Y. Chevalier, S. Briançon, L. Beney, H. Fessi, *J. Colloid. Interface Sci.*, **2008**, *317*, 458.

[20] C. Pinto, R. J. Neufeld, A. J. Ribeiro, F. Veiga, *Nanomedicine NBM*, **2006**, *2*, 8.

[21] M. V. Leroueil-Le, L. Fluckiger, Y. Kim, M. Hoffman, P. Maincent, *Eur J Pharm Biopharm*, **1998**, *46*, 137.

[22] A. Lamprecht, N. Ubrich, H. Yamamoto, U. Schäfer, H. Takeuchi, C. M. Lehr, P. Maincent, Y. Kawashima, *J. Control. Release*, **2001**, *71*, 297

[23] M. Chorny, I. Fishbein, H. D. Danenberg, G. Golomb, *J Control Release*, **2002**, *83*, 389.

[24] E. Cauchetier, M. Deniau, H. Fessi, A. Astier, M. Paul, *Int. J. Pharm.*, **2003,** *250*, 273.

[25] A. Budhian, S. J. Siegel, K. I. Winey, *Int. J. Pharm.*, **2007**, *336*, 367.

[26] H. Fessi, J. P. Devissague, F. Puisieux, C. Thies and J. P. Devissaguet, US Pat., 5118528, 1988.

[27] H. Fessi, F. Puisieux, J. P. Devissaguet, N. Ammoury, S. Benita, *Int. J. Pharm.*, **1989**, *55*, R1–R4.

[28] A. M. de Oliveira, E. Jäger, A. Jäger, P. Stepánek, F. C. Giacomelli, *Colloid. Surface. A*, 2013, 436, 1092.

[29] M. C. Brick, H. J. Palmer, T. H. Whitesides, *Langmuir*, **2003**, *19*, 6367.

[30] J. Aubry, F. Ganachaud, J-P C. Addad, B. Cabane, *Langmuir*, **2009**, *25*, 1970.

[31] I. Y. Perevyazko, J. T. Delaney Jr., A. Vollrath, G. M. Pavlov, S. Schubert, U. S. Schubert, *Soft Matter*, **2011**, *7*, 5030.

[32] I. Y. Perevyazko, J. T. Delaney Jr., A. Vollrath, G. M. Pavlov, S. Schubert, U. S. Schubert, *Soft Matter*, **2011**, *7*, 5030.

[33] J. A. Dirksen, T. A. Ring, *Chem. Eng. Sci.*, **1991**, *46*, 2389.

[34] S. A. Vitale, J. L. Katz, *Langmuir*, **2003**, *19*, 4105.

[35] S. M. D'Addio, R. K. Prud'homme, *Adv. Drug Deliv. Rev.*, **2011**, *63*, 417.

[36] D. Horn, J. Rieger, *Angew. Chem.*, **2001**, *40*, 4330.

[37] L. Capretto, D. Carugo, S. Mazzitelli, C. Nastruzzi, X. Zhang, *Adv. Drug Deliv. Rev*, **2013**, *65*, 1496.

[38] M. E. Gindy, A. Z. Panagiotopoulos, R. K. Prud'homme, *Langmuir*, **2008**, *24*, 83.

[39] C. Zhang, V. J. Pansare, R. K. Prud'homme, R. D. Priestley, *Soft Matter*, **2012**, *8*, 86.

[40] K. Roger, M. Eissa, A. Elaissari, B. Cabane, Langmuir, **2013**, *29*, 11244.

[41] P. Dagtepe, V. Chikan, *J. Phys. Chem. C*, **2010**, *114*, 16263–16269.

[42] S. Stainmesse, A. M. Orecchioni, E. Nakache, F. Puisieux, H. Fessi, *Colloid Polym Sci*, **1995**, *273*, 505.

[43] S. Galindo, F. Puel, S. Briançon, E. Allémann, E. Doelker, H. Fessi, *Eur. J. Pharm. Sci.*, **2005**, *25*, 357.

[44] F. Ganachaud, J. Katz, *Chemphyschem*, **2005**, *6*, 209.

[45] O. Thioune, H. Fessi, J. P. Devissaguet, F. Puisieux, *Int. J. Pharm.*, **1997**, *146*, 233.

[46] P. Legrand P, S. Lesieur, A. Bochot, R. Gref, Raatjes W, Barratt G, Vauthier C. *Int. J. Pharm.*, **2007**, *344*, 33.

[47] S. Galindo-Rodriguez, E. Allémann, H. Fessi, E. Doelker, *Pharm. Res*. **2004**, *21*, 1428.

[48] J. Cheng, B.A. Teply, I. Sherifi, J. Sung, G. Luther, F.X. Gu, E. Levy-Nissenbaum, A.F. Radovic-Moreno, R. Langer, O.C. Farokhzad, *Biomaterials*, **2007**, *28*, 869.

5. Biocompatible and biodegradable polymeric nanoparticles for drug delivery

5.1 Introduction

The search for new biomaterials intended for biomedical applications has considerably intensified in recent years. The most promising applications are the ones focused on the development of controlled drug delivery systems.[1] The use of biocompatible and biodegradable polymers is very attractive because controlled drug release can be optimized by suitable degradation strategies and it allows clearance of the polymeric material from the body, avoiding its accumulation and possible toxicity.[2,3]

Among the FDA-approved polymers, polybutylene succinate (PBS) is also an important commercial available biodegradable aliphatic polyester derived from fatty C-4 compounds.[4,5,6,7] The absence of cytotoxic degradation products, e.g. succinic acid is an intermediate in the TCA cycle (tricarboxylic acid cycle, citric acid cycle) makes PBS copolyesters prospective candidates aiming the development of drug delivery structures.[8,9,10,11] Furthermore, the fatty acids (FA) such as dilinoleic acid (DLA) are suitable components to the preparation of biodegradable polymers since they are hydrophobic naturally occurring body compounds[12,13] and they are able to sustain encapsulated hydrophobic drugs via hydrophobic interactions when used as drug nanocarriers.[14,15,16,17]

Some of the potentialities of the combination of polybutylene succinate with fatty acids in the development of new materials for drug delivery applications are explored in this chapter. The aliphatic biodegradable copolyester named PBS/PBDL (poly(butylene succinate-co-butylene dilinoleate)) was synthesized by melt polycondensation and characterized by ^{1}H NMR, ^{13}C NMR, GPC, DSC and DLS.[15] The surfactant-free PBS/PBDL nanoparticles (NPs) were produced by using the single-step nanoprecipitation protocol (Chapter 4) and characterized by employing SLS, DLS, SAXS and transmission electron microscopy (TEM). The most relevant results related to the PBS/PBDL NPs are showed and discussed in this chapter. Methodological description and detailed discussion, when not mentioned in the chapter can be found in the appendices.

5.2 Nanoparticles characterization

The molecular structure of PBS/PBDL copolyester is shown in Fig. 5.1. The detailed information related to the copolyester synthesis and characterization is given in appendix II.

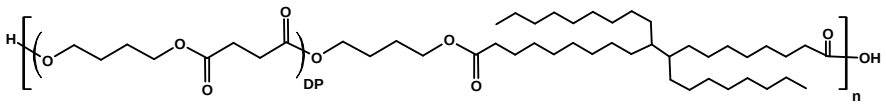

Figure 5.1. Molecular structure of poly(butylene succinate-*co*-butylene dilinoleate (PBS/PBDL) copolyester.

After evaporation of the organic solvent the PBS/PBDL NPs were investigated by using several scattering techniques (DLS, SLS and SAXS) and TEM.

Fig. 5.2 shows DLS results of the PBS/PBDL NPs prepared at different polymer concentrations. Fig. 5.2a shows the autocorrelation function measured at 90° and the respective normalized distributions of relaxation times $\tau A(\tau)$.

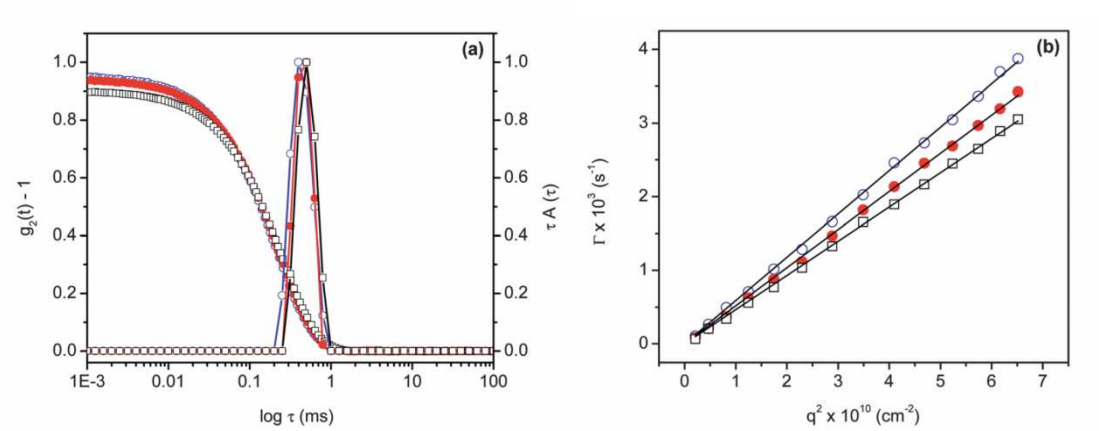

Figure 5.2. (a) Autocorrelation functions $g_2(t)$-1 measured at scattering angle 90° and the respective distributions of the relaxation times $\tau A(\tau)$ revealed by REPES analysis for PBS/PBDL NPs at starting polymer concentrations 2.5 mg.mL^{-1} (○), 5.0 mg.mL^{-1} (●) and 10 mg.mL^{-1} (□). (b) Variation of the relaxation frequency $\Gamma = 1/\tau$ as a function of q^2.

The diffusive behavior of the produced PBS/PBDL NPs is shown in Fig. 5.2b and was confirmed by the linear q^2 dependence of the decay rate (Chapter 3, equation 3.24). Table 5.1 shows the hydrodynamic radii (R_H) determined by the Stokes-Einstein equation (Chapter 3, equation 3.25). The distributions of relaxation times exhibit an unimodal particle size distribution with the sizes ranging from 34.5 to 56.7 nm (i.e. mean diameters from 69.0 to 113.4 nm) as the polymer concentration increases from 2.5 to 10 mg.mL^{-1}. The increase in nanoparticle size as a function of the polymer concentration is explained by the nucleation-

aggregation mechanism. An extensive and detailed discussion related to the nucleation-aggregation mechanism is presented in the chapter 4 (section 4.2.1).

The transmission electron microscopy (TEM) was used to confirm the formation of spherical nanoparticles (Fig. 5.3a). The size distribution histogram resulting from the image analysis[18] (Fig. 5.3b) gives a number average mean diameter (D_N, equation 3.34) and polydispersity index (P_{TEM}, equation 3.35) equal to 72.4 nm and 1.12, respectively (polymer concentration of 5 mg.mL^{-1}). Usually the particle sizes measured by TEM present smaller size values in comparison with those measured by DLS.[19] This difference in the particle size measurement was observed also here and is related to the size-distribution reported in each technique. DLS reports an intensity-average size distribution whereas TEM reports a number-average size distribution. Therefore, TEM images generally give lower values relative to DLS data.

Table 5.1. Physico-chemical characteristics of the produced PBS/PBDL nanoparticles.

Entry	$c_{polymer}$ (mg.mL^{-1})	R_H (nm)	R_G (nm)	R_G / R_H	$M_{w(NP)}$ (10^8 g.mol^{-1})	d (g.mL^{-1})	dispersity	ζ (mV)
NP1	2.5	34.5	40.5	1.17	0.78	0.38	0.067	-36.0
NP2	5.0	46.7	52.6	1.13	1.03	0.39	0.083	-37.0
NP3	10.0	56.7	59.0	1.04	1.74	0.35	0.094	-35.0

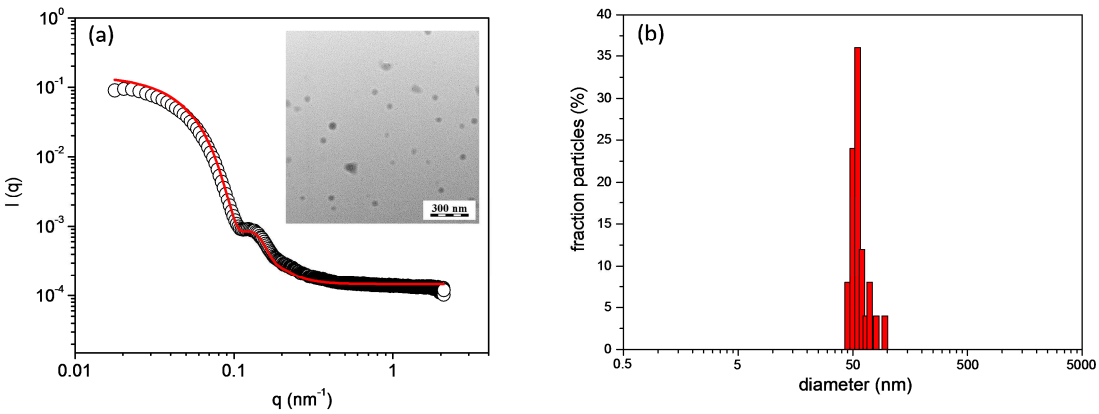

Figure 5.3. (a) SAXS data (circles) and corresponding curve fitting (red line) for PBS/PBDL nanoparticles produced from starting polymer concentration of 5.0 mg.mL^{-1}. The inset

portrays the TEM image in the same conditions. (b) Size distribution histogram of the TEM image of the PBS/PBDL nanoparticles.

SAXS measurements were also performed to probe the size of the PBS/PBDL nanoparticles and Fig. 5.3a shows a representative example. The resulting $I(q)$ vs. q scattering curves were fitted by using the form factor of homogeneous spheres and log-normal distribution for polydispersity. Detailed information related to the fitting procedures is described in the Chapter 3 (section 3.5) and the software used is described in appendix II. The fitting procedure provides a value of $D = 2R = 79.8$ nm and polydispersity (δ) of 0.144, which is in well agreement with the experimental data. It is also important to emphasize that the high quality of the fitting, particularly at the low-q range of the SAXS profile, indicates the absence of aggregating nanoparticles due to their electrostatic stabilization as discussed below.

SLS measurements were performed in order to investigate detailed information related to the physicochemical properties of PBS/PBDL NPs. The partial Zimm plot (appendix II, equation 2) results are reported in Fig. 5.4a (Table 5.1) and one example of the full Zimm plot (Chapter 3, equation 3.17) of NP3 PBS/PBDL NPs is showed in Fig. 5.4b. The very similar results allow the use of the partial Zimm plot version in which only one single concentration is used to perform the experiments. The partial Zimm analysis is only valid for very dilute solutions of strong scattering intensity.[20] The dn/dc value of the copolyester nanoparticles in water was experimentally measured (appendix II) and found to be equal to 0.153 mL.g^{-1}.

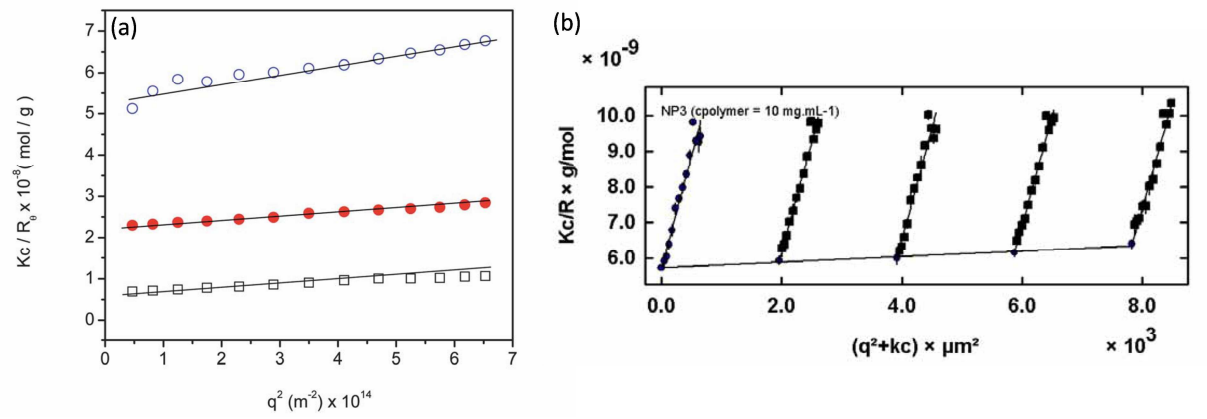

Figure 5.4. (a) Partial Zimm plot of static light scattering (Kc/R_θ vs. q^2) for PBS/PBDL nanoparticles prepared at 2.5 mg.mL^{-1} (○), 5.0 mg.mL^{-1} (●) and 10 mg.mL^{-1} (□) polymer concentrations. (b) Zimm plot of the sample NP3 (polymer concentration = 10 mg.mL^{-1}). For

the partial Zimm analysis the concentration of polymeric nanoparticles in all the samples was fixed at 0.1 mg mL^{-1} and for Zimm plot were 0.05, 0.1, 0.15 and 0.2 mg mL^{-1}.

Considering the reasons involved in the nucleation and aggregation mechanism (section 4.2.1, Chapter 3) the M_w of the PBS/PBDL NPs increases as a function of the polymer concentration (Table 5.1).

As previously mentioned in Chapter 3 (Section 3.3.3), the ρ-ratio (R_G/R_H) is an experimental quantity derived from the particle size characteristics determined from static (R_G, equation 3.17, Chapter 3) and dynamic light scattering measurements. It provides indication of the scattering particle conformation in solution. Regarding the polymer concentration, R_G/R_H values found for PBS/PBDL NPs within 0.977-1.127 (Table 5.1), is in the range for spherical nanoparticles made from regular branched polymer or statistical random polycondensates.[21,22,23] These values suggest that the particle structure follows the soft sphere model[21,24] and the assemblies contain high amounts of water entrapped inside.[24,25,26] The average density (d) of the NPs could also be determined using equation 3.33 (Chapter 3, section 3.8). The calculated d values of PBS/PBDL NPs within the range of 0.37-0.39 g.mL^{-1} (Table 5.1) are also a strong indication that the particles are water swollen. Furthermore, the water entrapment inside the PBS/PBDL NPs could explain the particle stability without addition of stabilizers. The water entrapment reduces the particles density and increases the surface charge. The particles negative ζ-potential (Table 5.1) was attributed to the presence of negative charges related to the carbonyl group in the ester bounds and to the remaining carbolxyl terminal groups in the surface of copolymer nanoparticles.[24,27,28]

5.3 Drug-loading and efficiency

The capacity of a nanocarrier to load a specific drug is given by the loading content (LC) and it is related to its mass (Chapter 3, equation 3.31) whereas the drug-loading efficiency (LE) is related to the total drug feeding (Chapter 3, equation 3.32). Therefore, an ideal nanoparticulate system should present high LC in order to reduce the quantity of polymer material for administration and a high LE to avoid drug losses during the therapy. In order to investigate the LC and LE of PBS/PBDL nanocarriers, paclitaxel (PTX) was used as the hydrophobic drug model and loaded to the copolyester NPs. The loading of the copolyester NPs with the drug was done using the nanoprecipitation procedure previously described except that in such a case known amount of PTX was dissolved in acetone with the

PBS/PBDL copolyester. The LC of the PBS/PBDL NPs was investigated in the range 1-10% $w_{drug}/w_{polymer}$ and the stability of the drug-loaded PBS/PBDL NPs was limited to ~ 6-7% $w_{drug}/w_{polymer}$ drug feeding. In order to compare the LE and LC of PBS/PBDL, two well-known FDA-approved polyesters (PLGA and PLA) were used to prepare PTX-loaded NPs. The drug feeding for all polyester NPs was preset to 2.5% $w_{drug}/w_{polymer}$. LC and LE found for PBS/PBDL were 2.5% $w_{drug}/w_{polymer}$ and 100 %, respectively. However, PLGA NPs presented a PTX LC of ~ 0.90% $w_{drug}/w_{polymer}$ and LE of ~89 % and for PLA NPs the LC and LE were ~ 0.73% and ~70%, respectively. The higher LC and LE values for PBS/PBDL copolyester suggest that this polymer presents stronger hydrophobic interactions with the PTX drug in comparison to PLGA and PLA polyesters. This is confirmed by the enthalpy values of the interaction parameter (χ_{dp}) between the PTX and the polyesters given by equation 1.1 (Chapter 1). The values of χ_{dp} for PLA, PLGA and PBS/PBDL were calculated from the respective solubility parameter of the polyesters (δ_p) and PTX (δ_d). The solubility parameters for PLA, PLGA and PTX were taken from literature[29,30,31] and for PBS/PBDL was estimated by using the group contribution method from Van Krevelen and Hoftyzer.[32] The χ_{dp} values found were 0.983, 1.328 and 0.0000287 for PLA, PLGA and PBS/PBDL, respectively. Therefore, these results indicate that PBS/PBDL copolyester nanoparticles are an interesting alternative for the encapsulation of hydrophobic drugs intended to biomedical and drug delivery applications.

5.4 Drug release experiments

In order to act on their target the drug molecules need to be dissolved in the aqueous environment in the body of the patient.[33,34] Therefore, it is expected that the nanocarrier releases the drug in a temporal controlled manner in the biological media. The temporal drug release in polyester nanoparticles is controlled by the drug diffusion from the polymeric matrix and from the polymer degradation.[33,35] The controlled diffusion release is dependent on the effective diffusion coefficient throughout the polymer matrix, which is related to the porosity and tortuosity.[36,37]

According to the stability of the drug-loaded PBS/PBDL NPs the release experiments were done by setting the loading content at LC = 5.0% $w_{drug}/w_{polymer}$. At this loading content the LE shows constant values of approximately 95%. The drug release as a function of time was monitored by HPLC and light scattering (DLS and SLS) and the results are shown in

Figure 5.5. It was found that approximately 40 % of the encapsulated PTX is released within the first 24 h whereas only 10% remains entrapped in the particles core after 120 h (Fig. 5.5a).

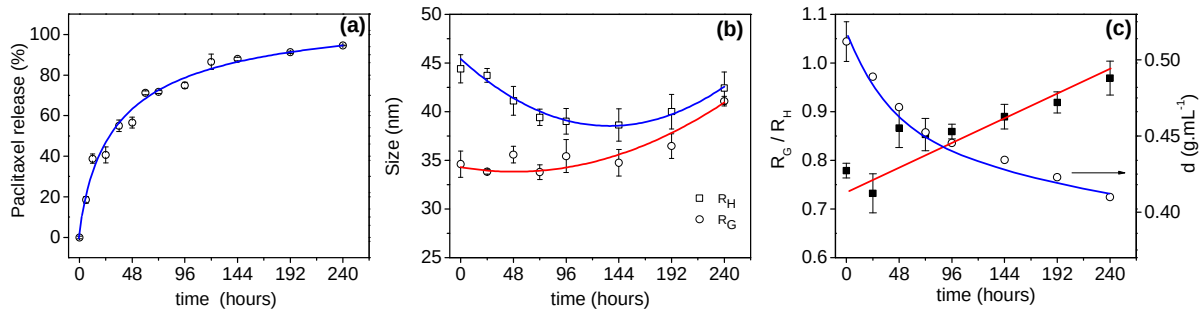

Figure 5.5. Drug release profile from PTX-loaded PBS/PBDL NPs prepared using $c_{polymer}$ = 5.0 mg mL^{-1} (a) R_G and R_H (b) and R_G/R_H and nanoparticle density (c) vs. time during PTX release.

The relative slow PTX release regime observed for the PBS/PBDL NPs might indicate that in this case the drug release is controlled by the diffusion of the drug through the polymer matrix and by the hydrolysis of the PBS/PBDL copolyester. Both parameters are related to the polymer hydrophobicity. It was observed that PLGA NPs loaded with PTX release more than 60% of the drug in 24 hours.[38] Taking into account the higher hydrophobicity of the PBS/PBDL copolymer in comparison to PLGA a slower release is expected of the PTX from the NPs prepared with the former copolyester. Moreover, the slower release of PTX in 24 h indicates that PBS\PBDL can sustain higher amounts of loaded drug in the circulation in comparison to PLGA. This increases the amount of the therapeutic drug in the target sites.

In order to follow the particles behavior during the drug release process DLS and SLS measurements were applied to the PBS\PBDL NPs loaded with PTX under release conditions (Fig. 5.5a and b). Additionally, besides DLS/SLS the drug encapsulation was also followed by SAXS measurements (Fig. 5.6). DLS/SLS and SAXS clearly indicate that the drug encapsulation reduces the dimensions of the NPs. The reduction observed in the hydrodynamic dimension R_H was from 46.7 (drug-free NPs, Table 5.1, $c_{polymer}$ = 5.0 mg.mL^{-1}) to 44.0 nm (drug-loaded NPs) whereas their radius of gyration (R_G) has been reduced from 52.6 to 35.0 nm. The observed reduction is more pronounced in R_G than in R_H. This reduction is reflected in the ρ value which decreases from 1.13 (drug-free NPs) to 0.79 (drug-laded NPs). Similar behavior was observed for SAXS of the unloaded and PTX-loaded NPs with

fitting the data using the form factor of homogenous spheres (Fig. 5.6). The reduction of the of the NPs the average radius (*R*) change from 39.9 (drug-free NPs) to 35.2 nm (drug-loaded NPs) confirms the results observed by light scattering.

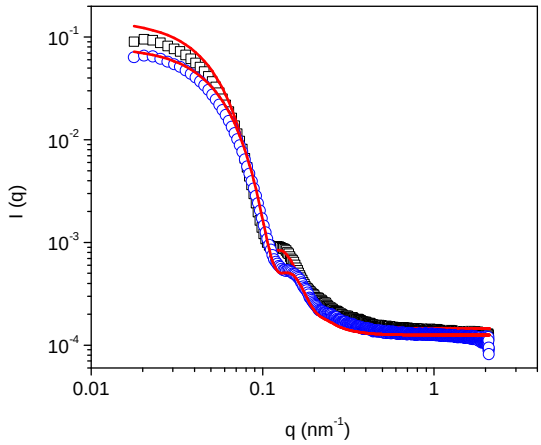

Figure 5.6. SAXS data (circles) and corresponding curve fitting (red line) for unladed (□) and 5.0 % $w_{drug}/w_{polymer}$ PTX-loaded (○) PBS/PBDL nanoparticles produced from starting polymer concentration of 5.0 mg.mL^{-1}.

Another interesting feature observed by DLS/SLS was the increase in the particles density from 0.39 to 0.51 g.mL^{-1} after the loading of PTX into the PBS/PBDL NPs. The increase in the NPs density associated with the reduction in the ρ-ratio (from soft to hard sphere) clearly reflects the transition of the inner particle structure from a water-swollen condition (drug free NPs) to a higher degree of compactness (drug-loaded NPs). The process involving the particles swelling-collapse induced by the PTX drug is schematically depicted in Fig. 5.7.

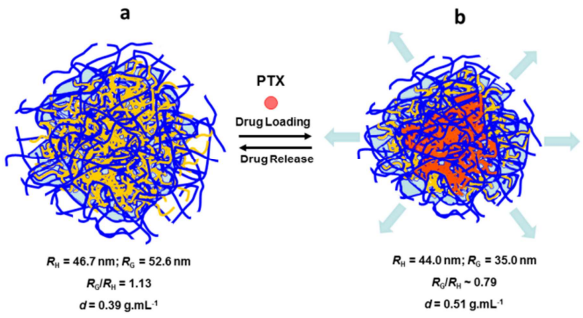

Figure 5.7. Schematic representation of the PTX-loading effect. Unloaded (a) and PTX-loaded PBS/PBDL NPs (b). The PTX drug is represented as filled circles and the islands of water are represented in blue.

However, in comparison to PBS/PBDL NPs loaded with PTX the PLA and PLGA nanoparticles loaded with 2% $w_{drug}/w_{polymer}$ presented an opposite behavior as reported in the table 5.2. It was observed an increase in R_G and R_H as PTX is loaded in the PLA and PLGA NPs. The increase was also confirmed by fitting the SAXS data of such systems (Figure 5.8) by using the form factor of homogeneous spheres. Although the NPs are more polydisperse, the shift towards the right-hand side of the $p(r)$ maximum as PTX is present fully confirms the size increase of the supramolecular aggregates (Fig. 5.8b and d). Furthermore, no changes in the PLA and PLGA NPs density could be detected after drug loading (Table 5.2). These differences observed between PLA and PLGA in comparison to PBS/PBDL NPs under the presence of PTX might be related to the hydrophobicity of the PBDL monomer units in the copolyester (Appendix III). The PBDL monomer unit, which is basically a branched hydrocarbon chain and therefore it is extremely hydrophobic, provides to the PBS/PBDL copolyester a much higher hydrophobic characteristic in comparison to PLA and PLGA polyesters. As aforementioned, under gest free conditions this is reflected in a much more compact and dense PBS/PBDL NPs in comparison to PLA and PLGA NPs (table 5.2). The interaction between the PBS/PBDL copolyester chains during the particle formation (nucleation-aggregation) might be stronger in comparison to PLA and PLGA polyester thus much more densely packed NPs are observed for PBS/PBDL. Taking into account that PTX is highly hydrophobic (water solubility ~ 0.1 μ/mL)[39] it is expected that its presence favors the interactions between PTX and PBS/PBDL chains leading to water draining out of the particles during the aggregation-nucleation process. Since the primary nuclei are more hydrophobic under the presence of PTX, larger amounts of water are draining out of the particle and their overall density increases. In the case of PLA and PLGA NPs the absence of a highly hydrophobic and flexible monomeric unit limits the strength of the hydrophobic interactions between the polymer chains as well as between the polymer and paclitaxel. This structural difference between the polyesters is reflected in a less densely packed and highly hydrated PLA and PLGA nanoparticles in comparison to the PBS/PBDL nanoparticles. Therefore, the addition of PTX to the PLA or PLGA nanoparticles system causes only an increase in the particles sizes (Table 5.2).

Table 5.2. Physicochemical characteristics of the guest-loaded NPs

Entry	R_H (nm)	dispersity[a]	ζ (mV)	$M_{w(NP)}$ (10^7 g.mol^{-1})	R_G (nm)	R_G/R_H	d_{NPs} (g.cm^{-3})	d [b] (*bulk polymer*)
PLGA	31.3	0.10	-37.0	1.7	26.7	0.85	0.06	1.34
PLGA 2.0%	38.2	0.12	-30.0	3.2	32.1	0.84	0.05	
PLA	32.1	0.10	-35.0	4.7	26.0	0.81	0.06	1.32
PLA 2.0%	34.7	0.11	-32.0	10.7	31.3	0.90	0.05	
PBSBDL	46.7	0.10	-37.0	10.3	52.6	1.13	0.39	1.08

[a] estimated by using the Cumulant method; [b] g.cm^{-3}

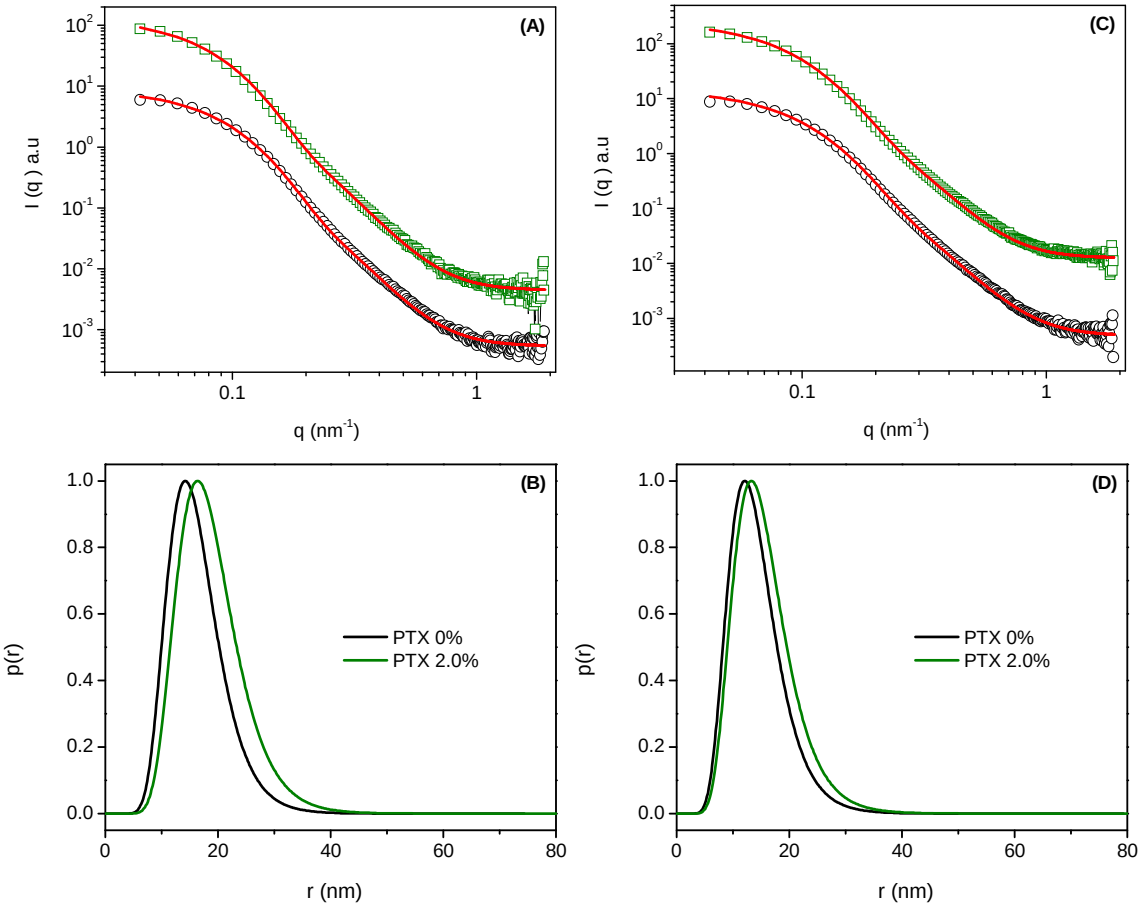

Figure 5.8. SAXS patterns of guest-free (○) and 2.0 % w_{PTX}/w_{PLA} guest-loaded NPs (○) (A) and respective $p(r)$ *vs*. r (B). Analogous data for PLGA NPs (C and D).

The result of the drug release from PBS/PBDLA nanoparticles followed by DLS/SLS is characterized by a continuous increase of R_G/R_H and decrease of nanoparticles density (Fig 5.5c). The increase in the R_G/R_H is mainly related to the reduction in the R_H since R_G remains nearly constant during the first half of the experiment. We observed a reduction of R_H within the first 96 h followed by a slight increase after 144 h (Fig. 5.5b). The initial reduction in R_H might be related to the PTX diffusion from the core of the PBS/PBDL NPs toward their surface. When PTX diffuses from the core in direction to the shell the water remaining drains towards the surface of the particle. This causes an increase in the hydrophobicity along the particles and to the shrinking of the polymer matrix which is experimentally observed by the reduction of the hydrodynamic dimension of the PBS/PBDL NPs during the first 96 h. In this case the PTX diffusion and water draining towards the surface of the particle are faster than water draining towards the core. Near the end of the experiment (after 192 h) the R_G increases and approaches the initial values (Fig. 5.5b) whereas the particles density decreases to ~ 0.41 $g.mL^{-1}$ (Fig 5.5c). The overall results suggest that the particles acquire their initial soft characteristics when the hydrophobic PTX is totally released once the inner core is again water-swollen due the reduction in its hydrophobicity caused by the drug release. These results show that the release of the PTX from PBS/PBDL NPs is mainly governed by drug diffusion and water draining through the polymer matrix.

5.5 Degradation behavior of the copolyester nanoparticles

An important prerequisite for a potential biomedical application of hydrophobic biodegradable polymers is the knowledge of their biodegradation behavior. Two main degradation mechanism can be involved, depending on relative rates of water diffusion into the polymer matrix and degradation of the polymer.[40,41] When the rate of polymer degradation is faster than the rate of water diffusion into the polymer matrix the mechanism is called surface degradation. On the contrary, when diffusion of water into the matrix is faster than polymer degradation and the whole matrix is affected by degradation and erosion, the process is called bulk degradation. Under biological conditions (*in vitro* and *in vivo*) the degradation of polyesters proceeds by random hydrolytic cleavage of ester linkages.[42,43] It was previously shown that PLA and PLGA nanoparticles degrade by bulk mechanism.[44,45] Therefore is expected that for the PBS/PBDL nanoparticles the water diffusion into the polymer matrix would be faster than the cleavage of ester bonds and the most probable mechanism will involve bulk degradation.

Figure 5.9 shows the results for the degradation of PBS/PBDL NPs when followed by SEC and DLS during 8 weeks. A constant decrease was observed of the weight-average molar mass during the first week followed by a pronounced reduction in the second week (Fig 5.9 a). During this period only slight changes in the nanoparticle size were observed by DLS (Fig 5.9 b). Starting after the second week a slower degradation profile was observed with smaller reductions in the molecular weight which persist until the end of the experiment. DLS measurements during this period show that at the end of the third week the nanoparticles collapsed and only aggregates were detected (Fig 5.9 b). Similar degradation profile was observed also for PLGA nanoparticles (~ 100 nm) prepared by double emulsion-solvent evaporation.[43] The authors claim that the initial fast loss in the molecular weight during the first weeks is related to the autocatalysis caused by the degradation products generated from the hydrolysis of the copolymer. The initial dense and compact structure of the polymer nanoparticles hinders and slows the outward diffusion of the degradation products, which can catalyze the degradation of the remaining polymer present in the particles. When the particles become more porous the diffusion of the degradation product is easier and the effect of autocatalysis vanishes. This might be the explanation for the fast degradation of the PBS\PBDL NPs since the particle density is higher in comparison to the PLGA NPs. In this case the outward diffusion of degradation products is expected to be even more hindered and therefore the autocatalysis effect is stronger.

The complete degradation process of the PBS/PBDL nanoparticles was followed by SEC (Fig. 5.9c). It was observed that the SEC curve shifts towards longer elution time as degradation proceeds. At the second week it was observed that the monomodal main peak starts to decompose into a bimodal distribution peak with is shifted to higher elution times (lower molecular weight) and the molar mass distribution becomes broader. These are clear indications of the presence of the degradation products with lower molecular weight (oligomers and monomers) derived from the hydrolytic cleavage of ester bonds.[46]

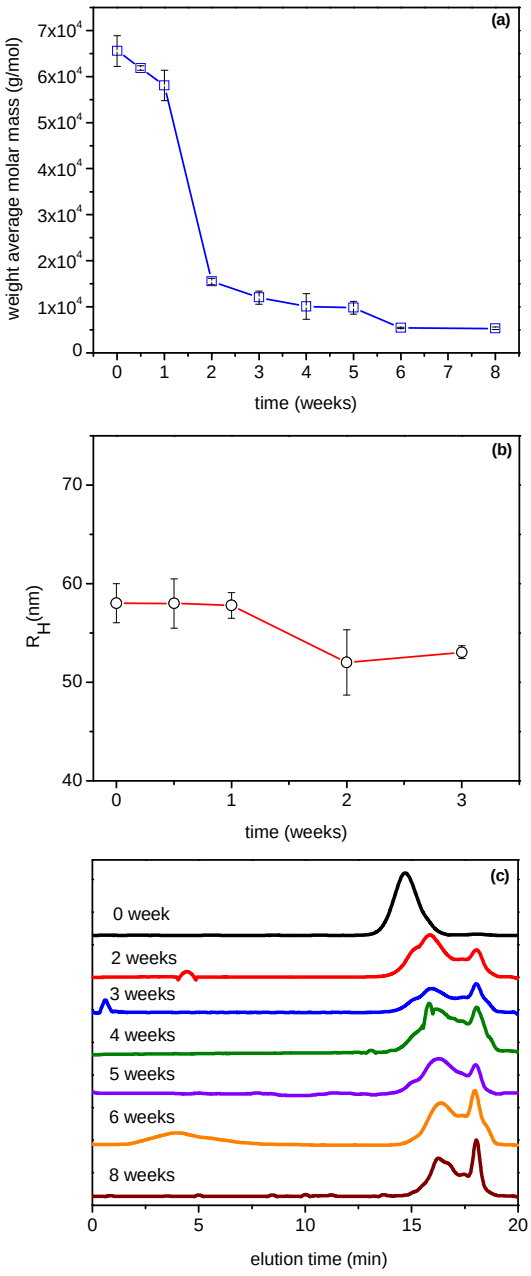

Figure 5.9. Weight-average molar mass (M_w) of polymers fragments (a), hydrodynamic radius (R_H) of the nanoparticles (b) as a function of time during incubation in PBS (pH 7.4) and respective SEC profiles (c).

5.6 In vitro cytotoxicity

The determination of cell viability *in vitro* is a crucial experiment in order to evaluate the cellular toxicity of a compound.[47] A toxic compound may initiate two distinct events: apoptosis or necrosis, two forms of cell death with clearly distinguishing morphological and biochemical features.[48] Therefore, the measure of the *in vitro* proliferation of the cells under the contact with the compound to be analyzed in function of time is a good indicator of its toxicity.

The in vitro cell proliferation was determined ref by incubation of the PBS/PBDL nanoparticles in mice splenocytes cell lines C57b/6 and Balb/c. The results show an increase in the cell proliferation which was concentration dependent for the NPs with both types of mice splenocytes cells evaluated (Fig. 5.10).

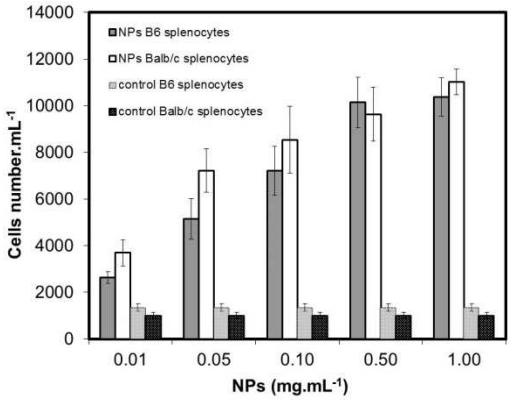

Fig. 5.10. *In vitro* effect of PBS/PBDL NPs (mg.mL^{-1}) on mice Balb/c and B6 splenocytes cell proliferation.

Similar dependence on the concentration in the cell proliferation was observed on surfactant-containing systems at low surfactant concentrations ref. However in this case, disruption of the cell membrane and high levels of cytotoxicity were observed at surfactant concentrations higher than 0.1 mg.mL^{-1}. In the current case, the enhanced in-cell proliferation was observed at much higher polymer concentration in comparison to those described for polymer surfactants. The most probable explanation for the increase in the cell proliferation is related to the metabolization of the fatty acids from the copolyester chains by the cells.[49] Weiss et al. observed similar *in vitro* behavior when steraoyl-poly(glycerol adipate) was incubated with human hepatoblastoma cells (HepG2).[50] The cell proliferation was observed

only when steraoyl was present in the poly(glycerol adipate) backbone. In this case the stearic acid fractions were primarily metabolized by the cells.

5.7 Conclusion

Novel biocompatible and biodegradable PBS\PBDL copolyester nanoparticles based on monomers derived from renewable sources were successfully produced. General characterization by TEM and SAXS reveals that the particles are spherical in shape and narrowly distributed. DLS measurements showing particles sizes around 120 nm indicates favorable conditions for drug delivery applications. Information related to the particle density and inner structure revealed by the combination of SLS and DLS measurements ($\rho = R_G/R_H$) suggest that they are water-swollen with a soft behavior. The water entrapped in the NPs seems to be crucial for the particle stability without surfactant. PBS/PBDL NPs were able to encapsulate between 3 to 5 times more hydrophobic drug PTX in comparison to the very well-known standard FDA approved polyester nanoparticles of PLA and PGLA. The drug encapsulation and release was followed by HPCL and for the first time by light scattering measurements (DLS and SLS). The drug encapsulation modifies the inner structure of the NPs leading to the shrinking and to higher degree of compactness due to hydrophobic interaction between the polymer and the drug. After the release of the drug the particles are swollen by water returning to their initial soft state. The degradability (about 8 weeks) and the absence of cell toxicity make PBS/PBDL NPs an interesting polyester alternative for biomedical applications in nanomedicine.

5.8 References

[1] J. R. Weiser, W. M. Saltzman, *J. Control. Release*, **2014**, *190*, 664.

[2] A. Díaz, R. Katsarava, J. Puiggalí, *Int. J. Mol. Sci.*, **2014**, *15*, 7064.

[3] C. S. Ha, J. A. Gardella Jr., *Chem. Rev.*, **2005**, *105*, 4205.

[4] H. Li, J. Chang, A. Cao, J. Wang, *Macromol. Biosci.*, **2005**, *5*, 433.

[5] J. Yang, W. Tian, Q. Li, Y. Li, A. Cao, *Biomacromolecules*, **2004**, *5*, 2258.

[6] I. Bechthold, K. Bretz, S. Kabasci, R. Kopitzky, A. Springer, *Chem. Eng. Technol.*, **2008**, *31*, 647.

[7] J. Xu, B.-H. Guo, "Microbial Succinic Acid, Its Polymer Poly(butylene succinate), and Applications", in *Plastics from Bacteria: Natural Functions and Applications*, Springer-Verlag Berlin, Heidelberg, 2010, p. 347.

[8] R. van Dijkhuizen-Radersma, J. R. Roosma, P. Kaim, S. Metairie, F. L. A. M. A. Péters, J. de Wijn, P. G. Zijlstra, K. de Groot, J. M. Bezemer, *J. Biomed. Mater. Res.*, **2003**, *67A*, 1294.

[9] R. van Dijkhuizen-Radersma, J. R. Roosma, J. Sohier, F. L. A. M. A. Péters, M. van den Doel, C. A. van Blitterswijk, K. de Groot, J. M. Bezemer, *J. Biomed. Mater. Res.*, **2004**, *71A*, 118.

[10] L. Wang, J. Chen, H. Liu, Z. Chen, Y. Zhang, C. Wang, Z. Feng, *Polym. Int.*, **2004**, *53*, 2145.

[11] A. Lindstrom, A. C. Albertsson, M. Hakkarainen, *Polym. Degrad. Stab.*, **2004**, *83*, 487.

[12] J. Bremer, H. Osmandsen, "Fatty acid oxidation and its regulation" in *New Comprehensive Biochemistry: Fatty acid metabolism and its regulation*, Elsevier, Amsterdam, 1984, p. 113.

[13] A. J. Domb, M. Maniar, *J. Polym. Sci. Part A Polym. Chem*, **1993**, *31*, 1275-1285.

[14] J. P. Jain, M. Sokolsky, N. Kumar, A. J. Domb, *Polym. Rev.* **2008**, *48*, 156-191.

[15] A. Jäger, D. Gromadzki, E. Jäger, F. C. Giacomelli, A. Kozlowska, L. Kobera, J. Brus, B. Rihova, M. El Fray, K. Ulbrich, P. Štěpánek, *Soft Matter*, **2012**, *8*, 4343.

[16] E. Jäger, A. Jäger, T. Etrych, F. C. Giacomelli, P. Chytil, A. Jigounov, J.-L. Putaux, B. Říhová, K. Ulbrich, P. Štěpánek, *Soft Matter*, **2012**, *8*, 9563.

[17] E. Jäger, A. Jäger, P. Chytil, T. Etrych, B. Říhova, F. C. Giacomelli, P. Štěpáanek, K. Ulbrich, *J. Control. Release*, **2013**, *165*, 153.

[18] J. Rieger, H. Freichels, A. Imberty, J.-L. Putaux, T. Delair, C. Jérôme, R. Auzély-Velty, *Biomacromolecules*, **2009**, *10*, 651.

[19] J. Tuoriniemi, A-C. J. H. Johnsson, J. P. Holmberg, S. Gustafsson, J. A. Gallego-Urrea, E. Olsson, J. B. C. Pettersson, M. Hassellöv, *Sci. Technol. Adv. Mater.*, **2014**, *15*, 035009.

[20] F. C. Giacomelli, I. C. Riegel, C L. Petzhold, N. P. da Silveira, P. Štěpánek, *Langmuir*, **2009**, *25*, 731-738.

[21] W. Burchard, K. Kajiwara, D. Nerger, *J. Polym. Sci., Polym. Phys. Ed.*, **1982**, *20*, 157–171.

[22] K. Kajiwara, *Polymer*, **1971**, *12*, 57–66.

[23] W. Burchard, in *Light Scattering from Polymers*, ed. W. Burchard, G D. Patterson, *Advances in Polymer Science*, 48, Springer-Verlag, New York, 1983; pp. 66–78.

[24] M. Seldák, Č. Koňák, *Macromolecules*, **2009**, *42*, 7430–7438.

[25] J. Fu, C. Wu, *J. Polym. Sci., Part B: Polym. Phys.*, **2001**, *39*, 703-708.

[26] J. Fu, X. Li, D. K. P. Ng, C. Wu, *Langmuir*, **2002**, *18*, 3843–3847.

[27] F. Quaglia, L. Ostacolo, G. De Rosa, M. I. La Rotonda, M. Ammendola, G. Nese, G. Maglio, R. Palumbo, C. Vauthier, *Int. J. Pharm.*, **2006**, *324*, 56–66.

[28] K. Roger, M. Eissa, A. Elaissari, B. Cabane, *Langmuir*, **2013**, *29*, 11244-11250.

[29] D. Karst, Y. Yang, *J. Appl. Polym. Sci.*, **2005**, *96*, 416–422.

[30] S. Schenderlein, M. Lück, B.W. Müller, *Int. J. Pharm.*, 2004, 286, 19–26.

[31] V. Kumar, R. K. Prud'homme, *J. Pharm. Sci.*, **2008**, *97*, 4904-4914.

[32] D. W. Van Krevelen, P. J. Hoftyzer, In *Properties of Polymers: Their Estimation and Correlation with Chemical Structure*; Elsevier: New York, 1976; p 129.

[33] K. E. Uhrich, S. M. Cannizzaro, R. S. Langer, K. M. Shakesheff, *Chem. Rev.*, **1999**, *99*, 3181, 3198.

[34] J. V. Natarajan, C. Nugraha, X. W. Ng, S. Venkatraman, *J. Control. Release*, **2014**, *193*, 122-138.

[35] J. M. Chan, L. Zhang, K. P. Yuet, G. Liao, J.-W. Rhee, R. Langer, O. C. Farokhzad, *Biomaterials*, **2009**, *30*, 1627–1634.

[36] E. Jager, C. G. Venturini, F. S. Poletto, L. M. Colome, J. P. U. Pohlmann, A. Bernardi, A. M. O. Battastini, S. S. Guterres A. R. Pohlmann, *J. Biomed. Nanotechnol.*, **2009**, *5*, 130–140.

[37] L. A. Fiel, L. M. Rebelo, T. M. Santiago, M. D. Adorne, S. S. Guterres, J. S. Sousa, A. R. Pohlmann, *Soft Matter*, **2011**, *7*, 7240–7247.

[38] C. Fonseca, S. Simões, R. Gaspar, *J. Control. Release*, **2002**, *83*, 273-286.

[39] T. Konno, J. Watanabe, K. Ishihara, *J. Biomed. Mater. Res.*, **2003**, 65A, 209–214.

[40] A. Göpferich, *Eur. J. Pharm. Biopharm.* **1996**, *42*, 1–11.

[41] F. von Burkersroda, L. Schedl, A. Göpferich, *Biomaterials*, **2002**, *23*, 4221–4231.

[42] C. G. Pitt, F. I. Chasalow, Y. M. Hibionada, D. M. Klimas, A. Schindler, *J. Appl. Polym. Sci.*, **1981**, *26*, 3779-3787.

[43] G. G. Pitt, M. M. Gratzl, G. L. Kimmel, J. Surles, A. Sohindler, *Biomaterials*, **1981**, *12*, 215-220.

[44] J. Panyam, M. M. Dali, S. K. Sahoo, W. Ma, S. S. Chakravarthi, G. L. Amidon, R. J. Levy, V. Labhasetwar, *J. Control. Release*, **2003**, *92*, 173-187.

[45] M. L.T. Zweers, G. H. M. Engbers, D. W. Grijpma, J. Feijen, *J. Control. Release*, **2004**, *100*, 347-356.

[46] I. Grizzi, H. Garreau, S. Li, M. Vert, *Biomaterials*, **1995**, *16*, 305-311.

[47] E. V. Komissarova, S. K. Saha, T. G. Rossman, *Toxicol. Appl Pharm.*, **2005**, *202*, 99-107.

[48] A. H. Wyllie, J. F. Kerr, A. R. Currie, *Int. Rev. Cytol.*, **1980**, *68*, 251-306.

[49] J. A. Ontko, *J. Biol. Chem.*, **1972**, *247*, 1788-1800.

[50] V. M. Weiss, T. Naolou, T. Groth, J. Kressler, K. Mäder, *J. Appl Biomater. Function Mater.*, **2012**, *10*, 163-169.

Publications

S. Petrova, C. G. Venturini, A. Jäger, E. Jäger, M. Hrubý, E. Pavlova, P. Štěpánek. Supramolecular self-assembly of novel thermo-responsive double-hydrophilic and hydrophobic Y-shaped [MPEO-*b*-PEtOx-*b*-(PCL)2] terpolymers. *RSC Advances*, under review.

S. Kazim, A. Jäger, M. Steinhart, J. Pfleger, J. Vohlídal, D. Bondarev, P. Štěpánek, Morphology and kinetics of aggregation of Ag nanoparticles induced with regioregular cationic polythiophene. *Langmuir*, under review.

A. Jäger, E. Jäger, F. C. Giacomelli, F. Nallet, M. Steinhart, J-L Putaux, K. Ulbrich, P Štěpánek, Shrinkage/Swelling of Polymeric Nanoparticles Induced by Hydrophobic Drug Entrapment. *Langmuir*, under review.

A. Jäger, E. Jäger, F. Surman, A. Höcherl, B. Angelov, K. Ulbrich, M. Drechsler, V. Garamus, C. Rodríguez-Emmenegger, F. Nallet P. Štěpánek. Nanoparticles of poly([*N*-(2-hydroxypropyl)]methacrylamide)-*b*-poly[2-diisopropylamino)ethyl methacrylate] diblock copolymer for pH-triggered release of paclitaxel. *Polymer Chemsitry*, **2015**, *6*, 4946-4954.

R. K. Donato, M. Lavorgna, P. Musto, K. Z. Donato, A. Jäger, P. Štěpánek, H. S. Schrekker, L. Matejka. The Role of Ether-Functionalized Ionic Liquids in the Sol-Gel Process. *J. Colloid Interf. Sci*, **2015**, 447, 77–84.

S. Petrova, C. G. Venturini, A. Jäger, E. Jäger, P. Černoch, S. Kereïche, L. Kováčik, I. Raška, P. Štěpánek. Novel thermo-responsive double-hydrophilic and hydrophobic MPEO-*b*-PEtOx-*b*-PCL triblock terpolymers: Synthesis, characterization and self-assembly studies. *Polymer*, **2015**, 59, 215-225.

M. Oliveira, B Mattei, K. Riske, A. Jäger, E. Jäger, P. Štěpánek, F. C. Giacomelli. Understanding the structural parameters of biocompatible nanoparticles dictating protein fouling. *Langmuir*, **2014**, 30, 9770-9779.

S. Petrova, E. Jäger, R. Konefał, A. Jäger, C.G. Venturini, J. Spěváček, P. Štěpánek. Novel poly(ethylene oxide monomethyl ether)-*b*-poly(ε-caprolactone) diblock copolymers containing a pH-acid labile ketal group as blocks linkage. *Polymer Chemistry*, **2014**, 5, 3884-3893.

P. Severino, T. Andreani, A. Jäger, M. V. Chaud, M. H. A. Santana, A. M. Silva, E. B. Souto. Solid lipid nanoparticles for hydrophilic biotech drugs: Optimization and cell viability studies (Caco-2 & HEPG-2 cell lines). *European Journal of Medicinal Chemistry*, **2014**, 81, 28-34.

E. Jäger, A. Jäger, P. Chytil, T. Etrych, B. Říhova, F.C. Giacomelli, P. Štěpánek, K. Ulbrich. Combination chemotherapy using core-shell nanoparticles through the self-assembly of HPMA-based copolymers and degradable polyester. *Journal of Controlled Release*, **2013**, 165, 153-161.

M. Oliveira, E. Jäger, A. Jäger, P. Štěpánek, F.C. Giacomelli. Physicochemical aspects behind the size of biodegradable polymeric nanoparticles: a step forward. *Colloids and Surfaces A: Physicochemical and Engineering Aspects*, **2013**, 436, 1092-1102.

F.C. Giacomelli, P. Štěpánek, V. Schmidt, E. Jäger, A. Jäger, C. Giacomelli. Light Scattering Evidences of Selective Protein Fouling on Biocompatible Block Copolymer Micelles. *Nanoscale*, **2012**, 4, 4504-4514.

E. Jäger, A. Jäger, T. Etrych, F.C. Giacomelli, P. Chytil, A. Jigounov, J-L. Putaux, B. Říhova, K. Ulbrich, P. Štěpánek. Self-assembly of Biodegradable Copolyester and Reactive HPMA-based Polymers into Nanoparticles as an Alternative Stealth Drug Delivery System. *Soft Matter*, **2012**, 8, 9563-9575.

A. Jäger, D. Gromadzki, E. Jäger, F. C. Giacomelli, A. Kozlowska, L. Kobera, J. Brus, B. Říhova, M. El Fray, K. Ulbrich, P. Štěpánek. Novel "soft" biodegradable nanoparticles prepared from aliphatic based monomers as a potential drug delivery system. *Soft Matter*, **2012**, 8, 4343-4354.

E. Penott-Chang, G. Mezzalira, P. Millard, A. Jäger, E. Jäger, A. H. E. Muller, S. S. Guterres, A. R. Pohlmann. Amphiphilic Diblock Copolymer and Polycaprolactone Blends to Produce New Vesicular Nanocarriers. *Journal of Biomedical Nanotechnology*, **2012**, 8, 272-279.

F. C. Giacomelli, P. Štěpánek, C. Giacomelli, V. Schmidt, E. Jäger, A. Jäger, K. Ulbrich. pH-triggered block copolymer micelles based on a pH-responsive PDPA (poly[2-(diisopropylamino)ethyl methacrylate]) inner core and a PEO (poly(ethylene oxide)) outer shell as a potential tool for the cancer therapy. *Soft Matter*, **2011**, 7, 9316-9325.

C. Rodriguez-Emmeneger, A. Jäger, E. Jäger, P. Stepanek, A. Bollogna-Alles, S. S. Guterres, A. R. Pohlmann, E. Brynda, *Colloids Surf., B Biointerfaces*, **2011**, *83*, 376-381.